Stem Cell Reports
Article

ISSCR

OPEN ACCESS

Thymic stromal lymphopoietin controls hair growth

Jessica L. Shannon,[1,2] David L. Corcoran,[3] John C. Murray,[1] Steven F. Ziegler,[4,5] Amanda S. MacLeod,[1,2,6] and Jennifer Y. Zhang[1,7,*]

[1]Department of Dermatology, Duke University, P.O. Box 103052, Durham, NC 27710, USA
[2]Department of Immunology, Duke University, Durham, NC 27710, USA
[3]Genomic and Computational Biology, Duke University, Durham, NC 27705, USA
[4]Benaroya Research Institute, Seattle, WA 98101, USA
[5]Department of Immunology, University of Washington, Seattle, WA 98195, USA
[6]Molecular Genetics and Microbiology, Duke University, Durham, NC 27710, USA
[7]Department of Pathology, Duke University Medical Center, Durham, NC 27710, USA
*Correspondence: jennifer.zhang@duke.edu
https://doi.org/10.1016/j.stemcr.2022.01.017

SUMMARY

Skin tissue regeneration after injury involves the production and integration of signals by stem cells residing in hair follicles (HFSCs). Much remains unknown about how specific wound-derived factors modulate stem cell contribution to hair growth. We demonstrate that thymic stromal lymphopoietin (TSLP) is produced in response to skin injury and during the anagen phase of the hair cycle. Intradermal injection of TSLP promoted wound-induced hair growth (WIHG), whereas neutralizing TSLP receptor (TSLPR) inhibited WIHG. Using flow cytometry and fluorescent immunostaining, we found that TSLP promoted proliferation of transit-amplifying cells. *Lgr5*^{CreER}-mediated deletion of *Tslpr* in HFSCs inhibited both wound-induced and exogenous TSLP-induced hair growth. Our data highlight a novel function for TSLP in regulation of hair follicle activity during homeostasis and wound healing.

INTRODUCTION

Hair follicles (HFs) are a defining feature of mammals and function as self-renewing miniature organs. Specifically, HFs harbor stem cells that control cyclic growth of hair follicles under homeostatic conditions and contribute to re-epithelialization of the interfollicular epidermis upon wounding (Blanpain and Fuchs, 2014; Gay et al., 2013; Ge et al., 2017; Greco et al., 2009; Ito et al., 2007; Jaks et al., 2008; Joost et al., 2018; Wang et al., 2017). The HF microenvironment controls the activation state of hair follicle stem cells (HFSCs) and supports continuous renewal of hair by cycling through phases of anagen (active hair growth), catagen (regression), and telogen (resting) (Abbasi and Biernaskie, 2019; Blanpain et al., 2004; Cotsarelis et al., 1990; Handjiski et al., 1994; Stenn and Paus, 2001). Loss of HFSC function results in the loss and/or inability to grow hair because of a variety of etiologies, such as chemotherapy and radiotherapy for cancer treatment, autoimmune-mediated destruction of HFSCs in alopecia areata, and stunted anagen cycles in androgenic alopecia (AGA) (Garza et al., 2011). Symptoms of hair disorders are multidimensional and can negatively affect psychological health, psycho-social relationships, and other factors that influence quality of life (Hunt and McHale, 2005; Saed et al., 2017). Factors released after wounding activate HFSC and epidermal progenitors to support hair cycling and epidermal repair (Abbasi and Biernaskie, 2019; Abbasi et al., 2020; Blanpain and Fuchs, 2014; Nelson et al., 2013). In fact, microneedle infliction of micro-injury is a common treatment to ameliorate hair loss in AGA, though the specific mechanisms responsible for microneedle-induced hair growth are not well understood (Fertig et al., 2018; Hou et al., 2017). Untangling how HFSCs mobilize during homeostatic hair cycling and wound regeneration will provide insights for regenerative approaches for these disease states.

Advances in epithelial stem cell biology have defined the contribution of stem cells expressing leucine-rich G protein-coupled receptor 5 (LGR5) in HF cycling under homeostatic conditions and after wounding (Jaks et al., 2008; Joost et al., 2018; Snippert et al., 2010; Wang et al., 2017). Furthermore, proliferation of a progenitor-like, intermediate population of transit-amplifying cells (TACs) are essential to form the inner HF lineages of the hair follicle during hair cycling and HF regeneration after injury (Hsu et al., 2011, 2014). However, it is unclear which specific factors are responsible for HFSC activation and TAC expansion. Prior research has focused largely on signaling networks involved in HFSC activation, such as the Sonic Hedgehog (SHH) and Wnt/β-catenin signaling pathways (Choi et al., 2013; Ito et al., 2007; Lim et al., 2018). Despite these efforts, it remains unclear how wound-derived factors regulate hair growth.

Physical abrasion and exposure to allergens or microbial products result in the production of "alarmins," such as interleukin (IL)-25, IL-33, and thymic stromal lymphopoietin (TSLP) by epithelial cells (Tao et al., 2017). Production of these cytokines triggers the activation of specific type 2 immune responses to promote tissue repair (Tao et al., 2017). Although they may work in synergy, "alarmins" have apparent pleiotropic roles in modifying the function of

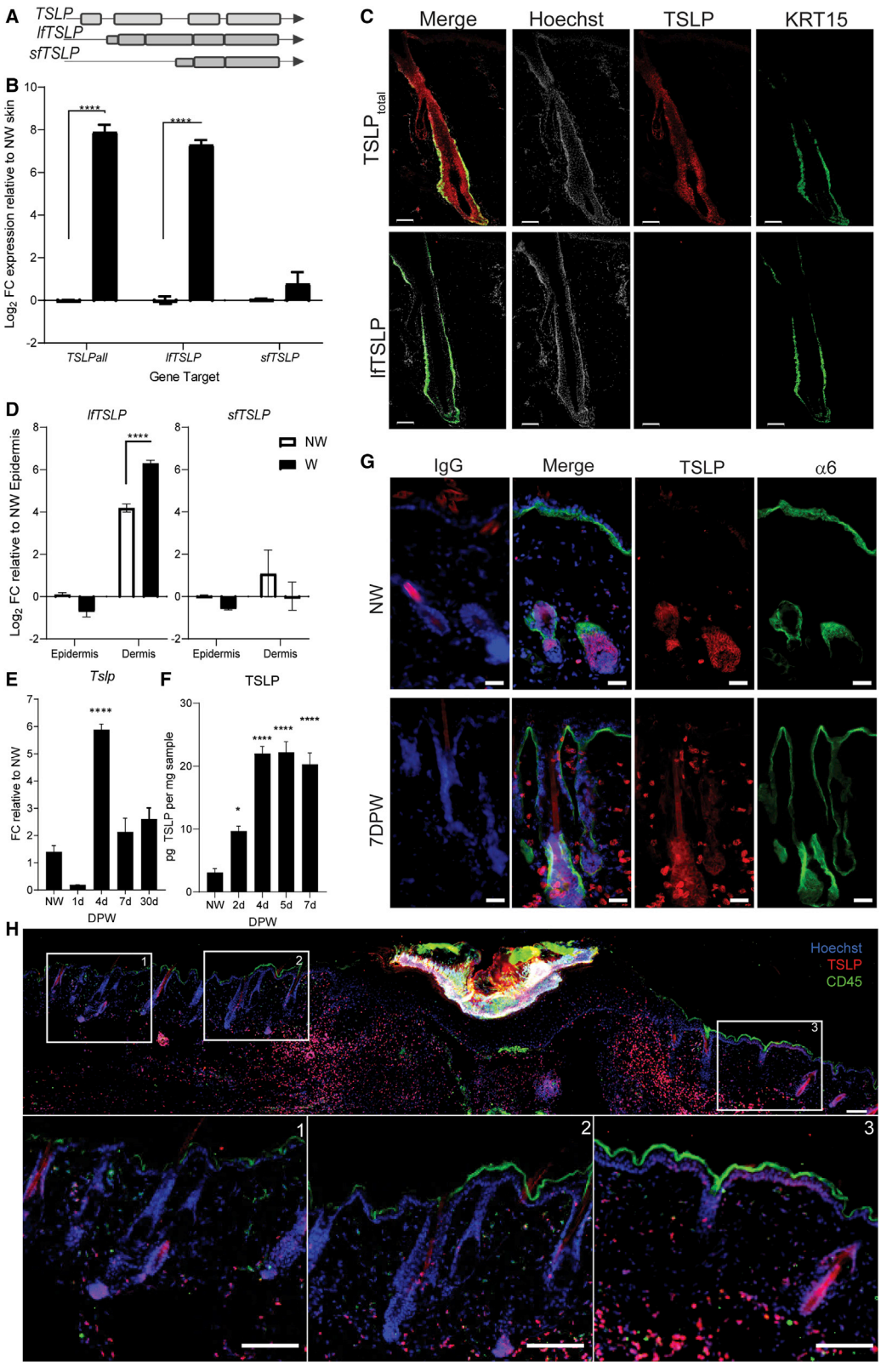

(legend on next page)

T cells, B cells, mast cells, neutrophils, and eosinophils in barrier tissues (Al-Shami et al., 2005; Kim et al., 2013; Rochman and Leonard, 2008; Salimi et al., 2013; Shane and Klonowski, 2014). TSLP and TSLP receptor (TSLPR) have been heavily studied in myeloid and lymphocyte compartments related to inflammatory conditions such as atopic dermatitis (Corren and Ziegler, 2019; Leyva-Castillo et al., 2013). The role of TSLP in the hair follicle microenvironment and its effect on epithelial cells remain largely unexplored.

In this study, we identified TSLP as a potent inducer of hair growth in response to skin injury. We show that local delivery of exogenous TSLP promotes hair growth both in the presence and absence of skin injury. Using *Lgr5*^{CreER}.*Tslpr*$^{fl/fl}$ mice, we demonstrate that TSLP acts through TSLPR on LGR5^{+} keratinocytes to promote expansion of TACs both during wound healing and normal tissue homeostasis. Furthermore, we found that TSLP increased expression of the cell cycle regulator cyclin D1 and the progenitor factor DDX6 in a TSLPR-dependent manner. Our findings delineate TSLP as a novel and locally produced cytokine that directly stimulates hair follicle cell proliferation in the skin.

RESULTS

TSLP is produced in the skin in response to injury

There are two variants of human TSLP whose expression is dictated by two putative promoter regions with different open reading frames that share a C-terminal region (Figure 1A) (Fornasa et al., 2015). Long-form TSLP (*lfTSLP*) is linked to type 2 immune responses and is highly induced in pathological conditions such as allergic diseases (Fornasa et al., 2015; Kim et al., 2013). Short-form TSLP (*sfTSLP*) is absent in mice but constitutively expressed in human epidermis (Bjerkan et al., 2015). Using quantitative reverse transcription PCR (qRT-PCR) with primers designed to discriminate between the two variants, we found that only *lfTSLP* was consistently upregulated in human skin 24 h after scratch wounding *ex vivo* (Figure 1B). To distinguish lfTSLP from sfTSLP at the protein level, we generated lfTSLP-specific polyclonal antibodies targeting the N-terminal region unique to lfTSLP. We validated the specificity of the lfTSLP antibody and confirmed upregulation of lfTSLP in atopic dermatitis lesions using immunofluorescence (Figure S1A), which is in agreement with previous findings (Imai, 2019; Islam and Luster, 2012; Kim et al., 2013; Salimi et al., 2013; Tao et al., 2017). lfTSLP was undetectable in healthy human skin, but TSLP$_{total,}$ as detected by the antibody that recognizes both variants, was abundantly expressed in the hair follicle (Figure 1C) and epidermis (Figures S1B and S1C), indicating that sfTSLP, but not lfTSLP, is expressed in the normal skin. qRT-PCR analysis of enzymatically separated epidermal and dermal parts of wounded skin revealed that lfTSLP was most significantly upregulated in the dermal part that contained dermis and hair follicles of both human (Figures 1D, S1D, and S1E) and mouse skin (Figure S2A). Interestingly, TSLP expression was largely restricted to hair follicles, sebaceous glands, and sweat glands in normal human skin, as shown by immunostaining (Figures S1B–S1E). Analysis of TSLP expression across different murine tissues revealed that TSLP expression was highest in the skin compared with other tissues, including lymphoid organs (Figures S2B and S2C).

TSLP functions via its heterodimeric receptor, composed of TSLPR (encoded by *Crlf2*) and IL7Ra; the receptor complex is highly conserved between human and mouse (Al-Shami et al., 2005; Fornasa et al., 2015; Leyva-Castillo et al., 2013; Verstraete et al., 2017; Wilson et al., 2013). Through analysis of existing transcriptomic datasets of full-thickness healing mouse wounds (Chen et al., 2010), we noted that *Tslp*, *Il7ra*, and *Crlf2* were all increased after wounding (Figure S2D). Consistently, qRT-PCR-based time course analysis revealed that *Tslp* mRNA peaked at about

Figure 1. TSLP is produced in the skin in response to injury

(A) Schematic illustration representing locus for human *TSLP*.

(B) qRT-PCR analysis of *TSLP* variants in human skin 24 h after wounding. Data presented are from 4 independent experiments using 4 different human donors in technical duplicates.

(C) Immunostaining human skin of TSLP$_{total}$ or long-form TSLP (lfTSLP; red) and KRT15 (green). Images presented are representative of 3 independent experiments using 3 different human donors. Scale bar: 100 μm.

(D) qRT-PCR analysis of *lfTSLP* and *sfTSLP* of human skin 24 h after *ex vivo* wounding. Data are from technical duplicates or triplicates of 4 experiments using 4 different human donors.

(E) qRT-PCR analysis of *Tslp* in RNA isolated from healing back skin wounds normalized to NW. Data are from 3 independent experiments, 4 pooled wounds per animal, n = 3 mice (NW, 4 DPW, 30 DPW) or n = 6 mice (1 DPW, 7 DPW) in technical triplicates.

(F) ELISA of TSLP in whole-tissue lysates of skin wounds (2 independent experiments, n = 2 or 3 mice per group).

(G) Immunostaining for TSLP (red) and ITGα6 (green) in non-wounded skin (top) or 7 DPW (bottom) skin from WT C57BL6 female mice. Scale bar: 20 μm.

(H) Immunostaining for TSLP (red) and CD45 (green) 7 DPW. All scale bars: 100 μm.

**p < 0.01, ***p < 0.001, and ****p < 0.0001. Error bars represent ±SEM. FC, fold change; NW, non-wounded; W, wounded; DPW, days post-wounding. See also Figures S1 and S2.

4 days after wounding (Figure 1E). Analysis by ELISA verified that TSLP protein level remained elevated for at least 7 days after wounding (Figure 1F). We detected TSLP in telogen and early anagen hair follicles of non-wounded skin and in hair follicles of skin 7 days post-wounding (Figures 1G and 1H). As expected, TSLP is highly expressed the dermal cells that likely included fibroblasts and immune cells, as indicated by the positive immunostaining of TSLP in both $CD45^+$ and $CD45^-$ cell populations (Figures S2E and S2F). In addition, we found that TSLP is readily detected in hair follicle bulge and hair germs (Figure 1G). The notable expression pattern of TSLP in HF keratinocytes and surrounding stromal cells coinciding with anagen entry suggests that TSLP plays an important role in anagen induction during tissue regeneration.

TSLP is expressed throughout the hair cycle and accelerates the onset of wound-induced hair growth

Stem cells in hair follicles mobilize after injury and aid regeneration of hair follicles, sebaceous glands, and the epidermis (Blanpain and Fuchs, 2014; Blanpain et al., 2004; Ge et al., 2017; Hsu et al., 2014; Joost et al., 2018). In particular, skin injury triggers activation of stem cells in surrounding telogen hair follicles to enter into hair cycling, a phenomenon understood as wound-induced hair growth (WIHG) that begins 7 days post-wounding (Abbasi and Biernaskie, 2019; Chen et al., 2015; Ito et al., 2005; Rahmani et al., 2018). As wound-induced TSLP upregulation preceded WIHG initiation and persisted locally in the skin, we hypothesized that TSLP has an important role in hair cycle activation. We first profiled TSLP expression throughout the hair cycle following depilation-induced entry of anagen phase. We monitored hair cycling on the basis of skin pigmentation as a defined temporal criterion (Chase, 1954; Müller-Röver et al., 2001; Stenn and Paus, 2001) (Figure S3A). qRT-PCR and ELISA revealed that TSLP was upregulated throughout the hair cycle, reaching peak expression during mid-anagen, when hair follicles extend deeper into the tissue, and then downregulated to lowest expression during catagen (Figures 2A and 2B). TSLP immunostaining was most prominent in cells of the outer root sheath and in the hair follicle bulge during mid-anagen (Figure 2C). In contrast, *Crlf2* and *Il7ra* expressions did not exhibit significant changes throughout the hair cycle (Figures 2A andS3B). To further determine *Tslp* transcriptional changes in wound-induced hair cycles, we wounded mouse skin in synchronized telogen and anagen phases and collected tissues 5 days after wounding. As expected, *Tslp* expression increased in response to injury and peaked in anagen skin; however, wounding anagen skin did not exhibit added effects to the already elevated *Tslp* expression (Figure S3C). These data suggest that TSLP functions locally in the hair follicle microenvironments to promote tissue regeneration.

The dynamic pattern of TSLP expression in hair cycling and response to skin injury led us to reason that TSLP may have a functional role in WIHG onset. We predicted that TSLP accelerates hair follicle cell proliferation, leading to expedited hair growth. To test this idea, we administered recombinant TSLP directly to the wound bed of small (4 mm diameter) and large (12 mm diameter) excisional punch wounds at the time of wounding. We found that wounds treated with TSLP consistently showed accelerated WIHG, as measured by the area of skin that entered anagen (Figures 2D, 2E, and S3D–S3F). Next, we interrupted TSLPR signaling using neutralizing antibodies (nAbs) administered directly to the wound bed immediately after wounding and again 4 days after wounding. TSLPR nAb-treated mice showed reduced hair growth compared with the IgG control (Figures S3G and S3H). Together, these data indicate that exogenous TSLP is sufficient and required for driving WIHG in large and small full-thickness wounds.

We next examined tissue sections from 13-day-old wound beds treated with 100 ng TSLP or 0.01% BSA in PBS to determine how TSLP altered behavior of hair follicle and other skin cells. TSLP-treated tissue showed morphological changes indicative of anagen entry 13 days after wounding and increased expression of the cell proliferation marker Ki67 compared with that of the control group (Figures 2F–2H). Similarly, TSLP treatment resulted in increased hair follicle length, epidermal thickness, and diameter of the hair follicle bulge (Figures 2H and S3I). Thus, TSLP delivery to wounds increased cellular proliferation and accelerated hair cycle entry into anagen and growth.

TSLP expands the $CD34^+ITG\alpha6^{lo}$ transit-amplifying cell population

Next, we sought to determine whether TSLP is sufficient to drive hair cycling in the absence of injury. Mice were given subcutaneous (s.c.) injections of recombinant TSLP or vehicle control at second telogen (Figure 3A). TSLP treatment alone was sufficient to drive hair cycling in wild-type (WT) mice (Figures 3B and 3C); interestingly, s.c. TSLP treatment resulted in hair growth temporally consistent with normal wound-induced hair growth. These findings lead us to postulate that hair follicle stem cells were directly responsive to local TSLP. To this end, we treated mice with TSLP and, 7 days later, pulsed animals with 5-ethynyl-2′-eoxyuridine (EdU) for 2 h to label proliferating cells. We then collected tissues and analyzed the frequency of cells expressing stem cell markers of the hair germ (LGR5), hair bulge (CD34), and EdU incorporation (Figure 3D). Fluorescence-activated cell sorting (FACS) analysis confirmed that TSLP treatment resulted in the expansion of $LGR5^+$ HFSCs, $CD34^+$ progenitors, and total EdU^+ cells

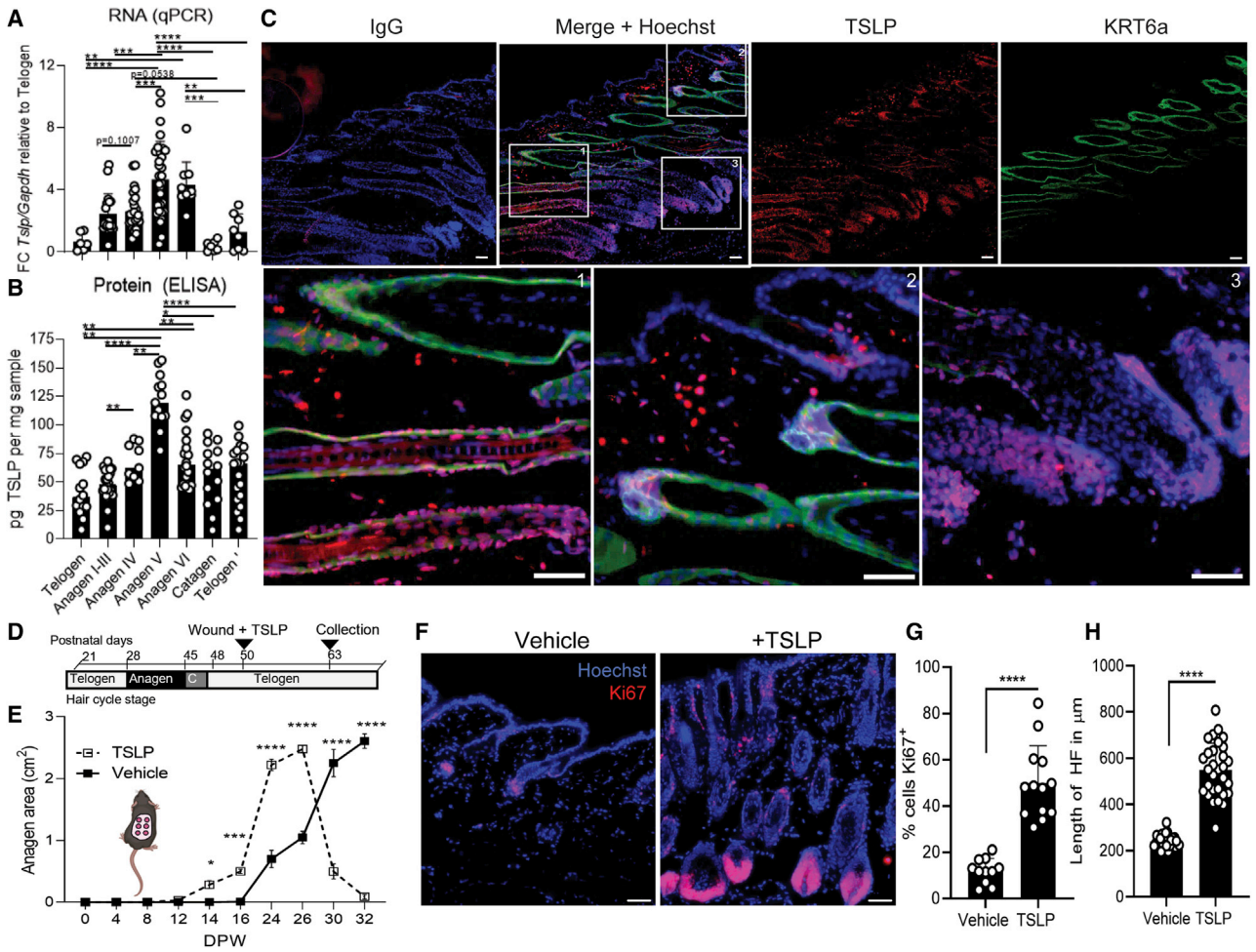

Figure 2. TSLP is expressed throughout the hair cycle and accelerates onset of wound-induced hair growth

(A) *Tslp* expression by qRT-PCR. Data represent 10–31 mice per group from 4 independent experiments. "Telogen" denotes telogen following a complete hair cycle.

(B) TSLP concentration in skin tissue by ELISA. Data represent 9–24 mice per group from 4 independent experiments.

(C) Immunostaining of skin samples collected from mice in anagen 8 days after depilation. Red, TSLP; green, KRT6a; blue, nuclei. Scale bars: 100 μm.

(D) Experimental timeline indicating hair follicle stages and treatments of vehicle (0.01% BSA) or recombinant mouse TSLP (100 ng/wound) following 4 mm punch biopsy.

(E) Quantification of skin area that entered anagen; represents data from 3 experiments using n = 8 mice per group.

(F–H) Immunostaining for Ki67 (F), (G) Ki67 quantification, and (H) hair follicle length measurement from mouse skin 13 days after wound and treatment with vehicle or TSLP. Data are from 2 experiments using n = 3 mice per group; 11–30 images per group were analyzed. Scale bars: 50 μm.

Error bars represent ± SEM. *p < 0.05, **p < 0.01, ***p < 0.001, and ****p < 0.0001. See also Figure S3.

(Figures 3E–3G and S4A–S4E). Interestingly, EdU^{+} cells were enriched in the CD34^{+}ITGα6^{lo} population (Figures 3H–3K), previously characterized as TAC cells (Hsu et al., 2014).

Two distinct CD34^{+} stem cell populations exist within the hair follicle, distinguished by expression intensity of integrin α6 (ITGα6); lower levels of ITGα6 indicate suprabasal positioning of cells derived from basal progenitors and higher levels of ITGα6 mark cells attached to the basement membrane (Barker et al., 2010; Blanpain et al., 2004). CD34^{+}ITGα6^{lo} cells are early progeny of ITGα6^{hi} basal bulge stem cells (Blanpain et al., 2004). Both CD34^{+}ITGα6^{hi} and CD34^{+}ITGα6^{lo} cells manifest self-renewal properties of stem cells: they withstand multiple passages in tissue culture *ex vivo* and can give rise to interfollicular epidermis and hair (Blanpain et al., 2004; Morris et al., 2004). By stratifying CD34^{+} cells by ITGα6 expression, we observed that

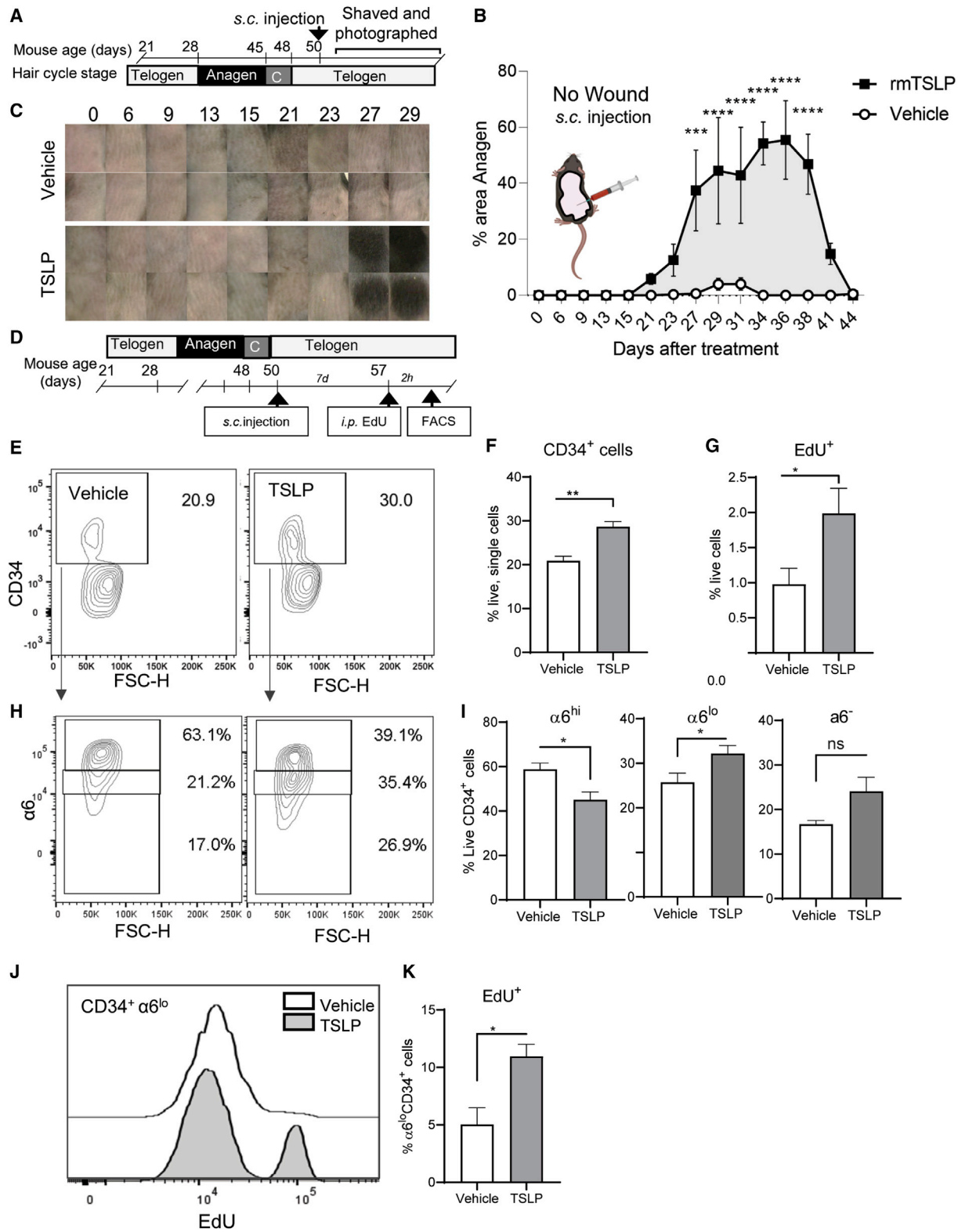

Figure 3. TSLP expands CD34$^+$ITGα6^{lo} transit amplifying cells (TACs)

(A) Experimental timeline for hair growth analysis following s.c. TSLP (250 ng).

(B) Quantification of skin area that has entered anagen. Data are from n = 3 mice per group.

(legend continued on next page)

TSLP-treated skin contained a unique CD34^{+}ITGα6^{lo} cell population that was not present in the vehicle-treated skin (Figures 3H, 3I, and S4F). Further analysis of this ITGα6^{lo} cell population revealed increased EdU incorporation, indicating that the CD34^{+}ITGα6^{lo} cells are highly proliferative compared with CD34^{+}ITGα6^{hi} and CD34^{-} cells (Figures 3J, 3K, and S4E–S4L). Together, these results indicate that TSLP drives the amplification of TACs, highlighting TSLP as a core growth factor of HF niche.

Murine epithelial cells express TSLPR

We next sought to identify cell types that mediate accelerated hair growth in response to TSLP. Flow cytometry analysis of tissues revealed that hair follicles were enriched with TSLPR^{+} cells compared with whole skin (Figures 4A–4C). Immunostaining of 7 day skin wound beds revealed that cells in wound-adjacent hair follicles expressed TSLPR (Figures 4D and 4E). As TSLP is a cytokine with immunomodulatory function, we asked whether TSLPR expression changes occur in immune cells and keratinocytes during wound healing. We used flow cytometry to quantify TSLPR expression in CD45^{+} immune and CD45^{-} non-immune cell compartments. Unexpectedly, we found that TSLPR expression was greatest on CD45^{-} cells in hair follicles of non-wounded tissue and that the CD45^{-}TSLPR^{+} cell population expanded during wound healing (Figures 4F and S5). We then performed immunostaining to determine the spatial orientation of TSLPR^{+} cells around the wound bed and in non-wounded telogen skin. TSLPR expression was localized largely to the outer root sheath of the hair follicle in both non-wounded and wounded skin, though wounded skin also exhibited strong TSLPR staining in the leading edge of the epidermis in comparison with non-wounded epidermis (Figures 4G and 4H). Notably, LGR5^{+} progenitors in the hair follicle contribute to the leading wound edge during tissue regeneration (Joost et al., 2018). The strong TSLPR signal on epithelial cells in and around the hair follicle bulge area suggests a role for TSLPR in hair follicle responses to injury.

TSLPR expression in LGR5^{+} HFSC is essential for WHIG

Given the positive expression of TSLP and TSLPR in epidermal stem cell compartments, we hypothesized that TSLP acts directly on HFSC to expand the TAC compartment. To test this hypothesis, we crossed *Lgr5^{CreER}* mice with *Tslpr$^{fl/fl}$* mice. Epithelial cell-targeted ablation of *Tslpr* was achieved by 4 consecutive daily topical treatments of 4-hydroxytamoxifen (4OHT) and confirmed by flow cytometry, which showed significant knockdown of TSLPR expression in LGR5^{+} cells (Figures 5A–5E and S6A), but not in CD45^{+} hematopoietic cells (Figures 5F and 5G). We did not detect a difference in the frequency of LGR5^{+} cells in 4OHT-induced mutant mouse skin compared with littermate controls, indicating that TSLPR loss did not deplete LGR5^{+} stem cell population. To address whether LGR5^{+} cells require TSLPR for WIHG, we treated *Lgr5^{CreER}.Tslpr$^{fl/fl}$* mice and their littermate controls with topical 4OHT to induce *Tslpr* ablation prior to wounding at second telogen (Figure 5H, top). As expected, control mice showed hair growth by day 23; in sharp contrast, *Lgr5^{CreER}.Tslpr$^{fl/fl}$* mice did not exhibit signs of WIHG for at least 32 days after wounding (Figures 5H and 5I). We next sought to address whether TSLPR was essential for accelerated WIHG in response to exogenous TSLP (Figure 5J). To do this, we treated animals with three tropical doses of 4OHT and then wounded telogen skin along with TSLP treatment (Figure 5J). As expected, littermate controls exhibited WIHG 17 days after wounding (Figures 5J and S6B–S6D). In contrast, mutant skin wounds did not show WIHG until 23 days after TSLP treatment (Figures 5J and S6B–S6D). In agreement with the hair growth phenotype, cyclin D1, a key cell cycle regulator (Tetsu and McCormick, 1999), was increased in control wounds or non-wounded tissues treated with TSLP; deletion of *Tslpr* in HFSC markedly diminished cyclin D1 expression in TSLP-treated wounds (Figures S6E–S6F). Together, these data underscore that TSLP acts through TSLPR in HFSCs and TACs to promote WIHG and homeostatic hair growth in the absence of wound injury.

TSLP promotes accumulation of keratinocyte progenitor factor DDX6

After wounding, HFSCs and epidermal stem cells are activated to expand cell populations and migrate to regenerate skin appendages and fill the wound gaps (Ge et al., 2017;

(C) Representative photos of mouse back skin after s.c. TSLP treatment.
(D) Experimental timeline for analysis of TSLP-driven cell proliferation.
(E) Representative flow cytometry plots of CD34^{+} cells.
(F) Quantification of CD34^{+} cells pre-gated on live, single cells.
(G) Quantification of total, live, EdU^{+} cells.
(H) IFlow cytometry plots representing ITGα6 expression pre-gated on CD34^{+} cells.
(I) Quantification of CD34^{+}ITGα6 subpopulations.
(J) Flow cytometry histogram overlay of CD34^{+}ITGα6^{lo} cells from TSLP- and vehicle-treated groups.
(K) Quantification of EdU^{+}CD34^{+}ITGα6^{lo}. Graphs represent means of 2 experiments using 6–8 mice per group ± SEM.
*p < 0.05, **p < 0.01, ***p < 0.001, and ****p < 0.0001. See also Figure S4.

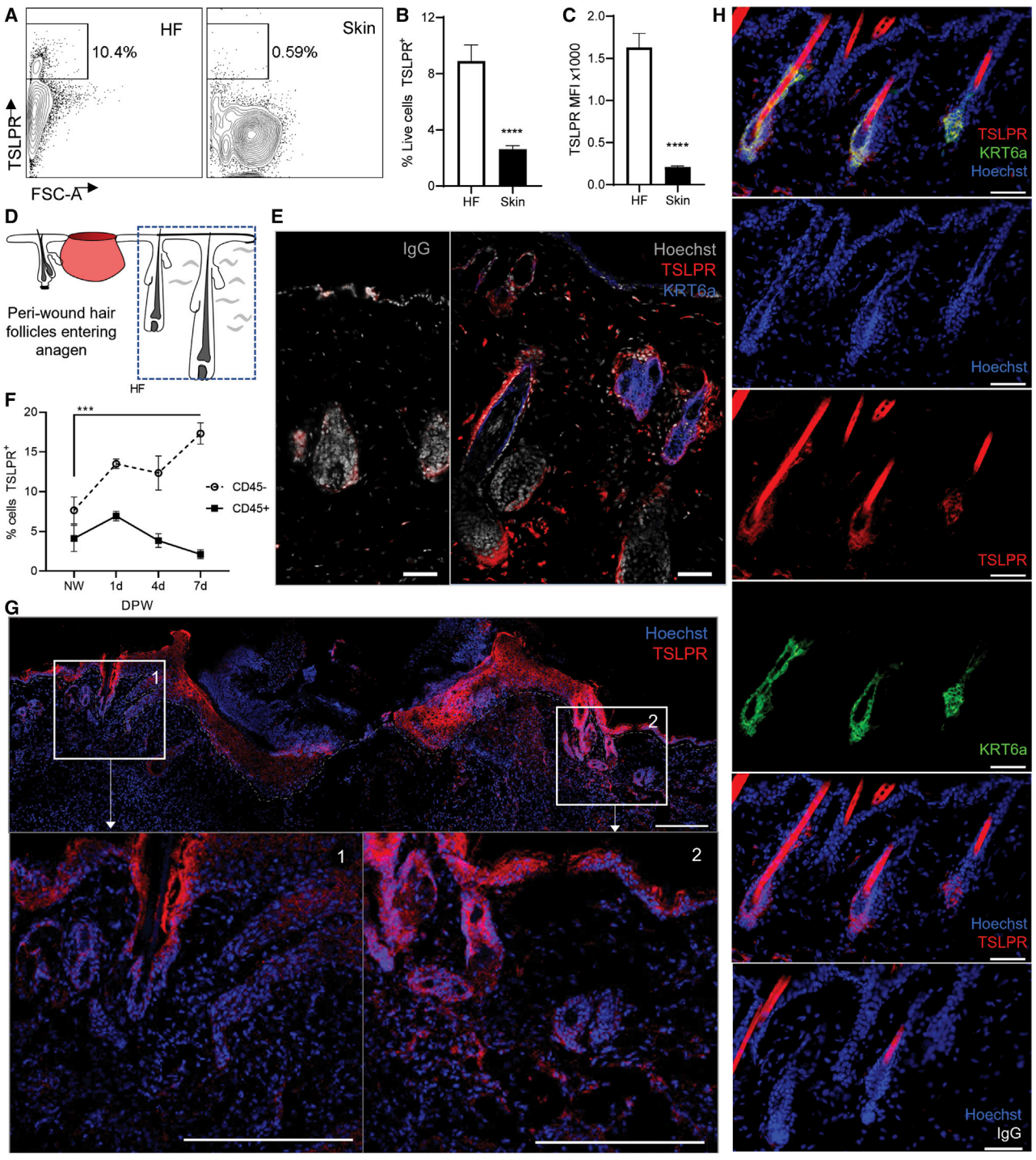

Figure 4. Murine epithelial cells express TSLPR

(A) Representative flow cytometry plots pre-gated on live, single cells.

(B) Quantification of TSLPR$^+$ relative cell abundance.

(C) Mean fluorescence intensity of surface expression of TSLPR on cells from hair follicle (HF) and skin from non-wounded tissue. Data presented represent averages ± SEM from 4 experiments using n = 7 mice (HF) and n = 20 mice (skin).

(D) Schematic showing location of tissue section portrayed in (E).

(E) Immunostaining of hair follicles neighboring 7-day-old wound bed. Red, TSLPR; blue, KRT6a. Scale bars: 50 μm.

(legend continued on next page)

Ito et al., 2007; Jensen et al., 2008; Levy et al., 2007). To determine additional molecular mechanisms mediating TSLP signaling in wound beds, we used a bioinformatics approach to identify differentially expressed genes (DEGs) that were upregulated in mouse skin treated with 3 μg s.c. TSLP continuously for 7 days using osmotic pumps (Christmann et al., 2013). We cross-referenced those genes with upregulated genes from small biopsy-induced normal healing wounds inflicted in mouse (Chen et al., 2010) or human (Iglesias-Bartolome et al., 2018) (Figure S8A; Table S1). Among the top shared DEGs was the upregulation of *DDX6*, which encodes an RNA helicase. Notably, DDX6 maintains epidermal stem and progenitor cell identities by suppressing translation of transcripts associated with keratinocyte differentiation programs such as KLF4 (Di Stefano et al., 2019; Wang et al., 2015).

We hypothesized that lfTSLP has a direct role on DDX6 transcription in human epidermal keratinocytes. We used qRT-PCR to measure transcriptional levels of DDX6 in primary normal human epidermal keratinocytes (NHEKs) treated with the recombinant human lfTSLP and sfTSLP. We found that lfTSLP treatment significantly increased expression of DDX6 by three-fold, whereas sfTSLP did not (Figure 6A). Consistently, KLF4 and Filaggrin (FLG), both of which are differentiation markers subject to downregulation by DDX6 (Wang et al., 2015), were decreased in cells treated by lfTSLP (Figure 6B). Furthermore, we confirmed that DDX6 was detectable at the protein level on immunofluorescence staining and observed increased formation of distinct DDX6 foci in response to lfTSLP (Di Stefano et al., 2019; Ostareck et al., 2014; Wang et al., 2015) (Figures 6C and 6D). To verify that TSLP directly alters proliferation of epidermal keratinocytes, we assessed phenotypic changes of cell proliferation marker Ki67 in epidermal keratinocytes following TSLP treatment. By flow cytometry, we found that treatment with lfTSLP but not sfTSLP resulted in keratinocyte proliferation, as evidenced by the increases in abundance and mean fluorescence intensity (MFI) of Ki67 (Figures 6E–6G). These data indicate that lfTSLP plays a dominant role in preserving keratinocyte stemness and promoting keratinocyte proliferation.

DISCUSSION

Our studies demonstrate that TSLP is sufficient to initiate hair cycle activation in quiescent hair follicles and accelerate hair growth after wounding. We report that TSLP is upregulated during the anagen phase of the hair cycle and following skin injury and peaks at about 4 days after wounding. We defined a novel function for TSLP acting on LGR5$^+$ cells and/or their progeny to promote generation of new hair follicles following skin injury. *Lgr5*^{CreER}-mediated genetic deletion of TSLPR or antibody-mediated biological blockade of TSLPR prior to wounding resulted in significantly delayed hair growth. We showed that TSLP drove generation of the TAC compartment *in vivo* and promoted keratinocyte proliferation *in vitro*. To our knowledge, a mechanism of TSLP regulation of hair growth by acting directly on hair follicle keratinocytes has not been described previously.

It has been well documented that TSLP is upregulated after injury in response to microbial products, skin distress signals, or inflammatory cytokines (Allakhverdi et al., 2007). TSLP is upregulated by airway epithelial cells and dendritic cells in response to TLR3 ligands, including double-stranded RNA, which may be released locally following physical trauma (Kato et al., 2007; Tanaka et al., 2009). Interestingly, TLR3$^{-/-}$ mice lack regenerative capacity compared with WT mice, indicating that TLR3 is crucial for wound-induced hair neogenesis (Bhoopalam et al., 2020; Garza et al., 2011; Kim et al., 2016, 2019; Nelson et al., 2013, 2015; Wier and Garza, 2020). However, it remains unknown whether TSLP-TSLPR signaling in skin wounds is coupled with or downstream of TLR3-depenent regeneration.

TSLP is expressed by various immune cells, including dendritic cells, mast cells, macrophages, eosinophils, and T cells (Al-Shami et al., 2005; He et al., 2008; Kim et al., 2013; Kubo et al., 2014; Oyoshi et al., 2010; Pandey et al., 2000; Reche et al., 2001). Our immunostaining suggests that keratinocytes are not the sole source of TSLP during homeostatic hair cycle and wounding healing and that additional immune and non-immune cells in the dermis contribute to local TSLP production. Emerging evidence has delineated TSLP functions in airway epithelial cell migration (Kabata et al., 2020), T_{Reg} expansion (Leichner et al., 2017), innate lymphoid cell activation (Kim et al., 2013), and sebaceous gland activity (Choa et al., 2021). We expect that TSLP exhibits pleiotropic activity beyond the known functions in the skin and other tissues. Although we did not observe significant changes in TSLPR$^+$CD45$^+$ cell populations in response to injury, we do not exclude that TSLP modulates immune cell function in the local tissue environment to favor hair growth.

(F) Flow cytometry for TSLPR$^+$ cells after wounding. Data are from 2 experiments using n = 2–4 mice per group in technical duplicates.
(G) Immunostaining TSLPR (red) of 7-day-old wound beds. Images 1 and 2 (insets) were enlarged to show detail. Scale bars: 200 μm.
(H) TSLPR immunostaining in non-wounded mouse back skin in telogen. Scale bars: 50 μm. Green, keratin 6a (KRT6a); blue, nuclei.
See also Figure S5.

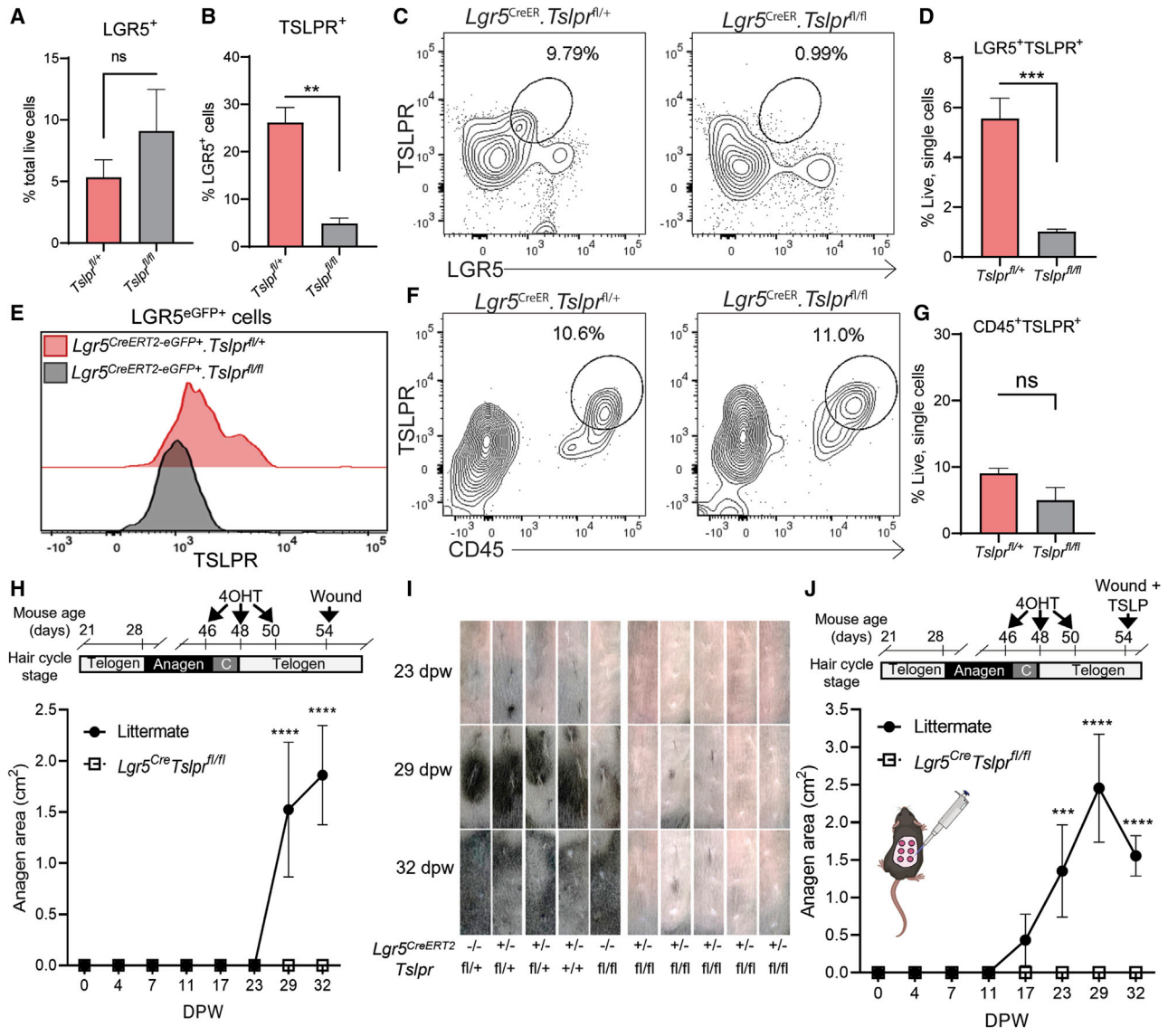

Figure 5. TSLPR expression by LGR5^{+} HFSCs is essential for WHIG

(A–G) Quantification of TSLPR^{+} cells by flow cytometry from *Lgr5^{CreER}.Tslpr$^{fl/fl}$* mice and *Lgr5^{CreER}.Tslpr$^{fl/+}$* mice treated daily for 3 consecutive days with 4-hydroxytamoxifen (4OHT). (A) LGR5-$^{eGFP+}$ cells pre-gated on total live cells. (B) TSLPR^{+} cells pre-gated on LGR5^{eGFP+} cells. (C) Flow plot and (D) quantification of TSLPR^{+}LGR5^{+} cells, pre-gated on live, single cells. (E) Histogram for TSLPR expression from total LGR5^{eGFP+} cells. (F) Flow cytometry plot and (G) quantification of TSLPR^{+}CD45^{+} cells, pre-gated on live, single cells. Data are from 2 independent experiments using 5–7 mice per group.

(H) Experimental timeline of quantification of skin that has entered anagen following wounding.

(I) Representative photos of mouse back skin after 4OHT treatment of *Lgr5^{CreER}.Tsfpr$^{fl/fl}$* and *Lgr5^{CreER}.Tslpr$^{fl/+}$* mice.

(J) Quantification of anagen skin area of mice treated with or without TSLP. Graph represents averages ± SEM of n = 4–6 mice per group across 3 experiments.

*p < 0.05, **p < 0.01, ***p < 0.001, and ****p < 0.0001. See also Figure S6.

It is reported that TSLP is negatively regulated by VDR and RXR signaling pathways and loss of RXR in epidermal cells results in type 2 skin inflammation in mice (Ganti et al., 2017; Li et al., 2005). K14-driven overexpression of TSLP in embryonic epidermal cells leads to skin inflammation in adult mice (Li et al., 2005). To our surprise, one dose of 100 or 250 ng TSLP into wounded or naive telogen skin was associated with neither inflammatory skin erosions nor delayed wound healing. Animals treated with this amount of TSLP did not exhibit

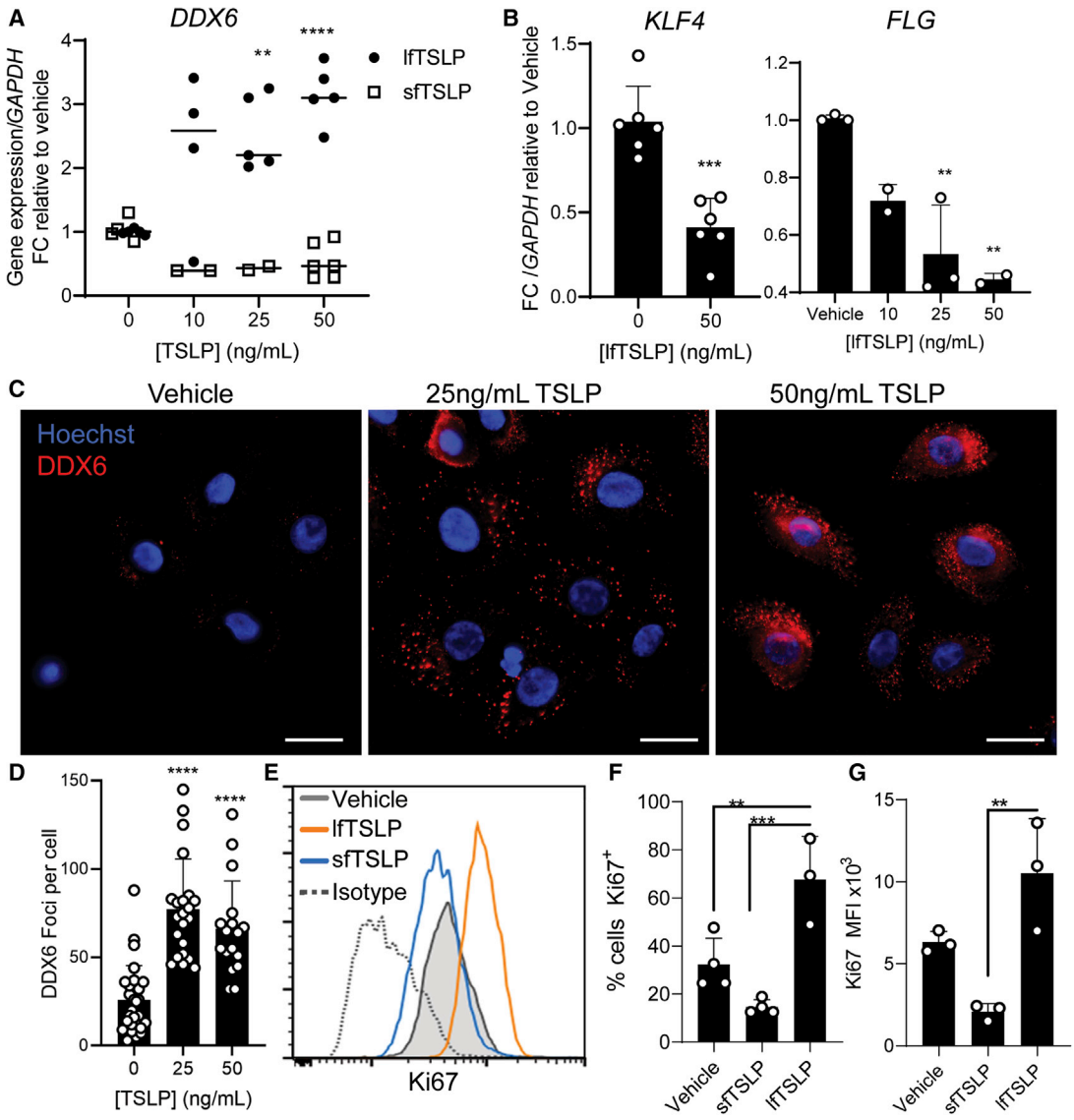

Figure 6. TSLP promotes accumulation of progenitor factor DDX6

(A and B) qRT-PCR analysis of *DDX6*, *KLF4*, and *FLG* of RNA isolated from primary human keratinocytes treated with sfTSLP or lfTSLP for (A) 16 h or (B) 24 h.

(C) Immunostaining of DDX6 (red) in primary human keratinocytes stimulated with human TSLP (100 ng/mL) for 20 h. Scale bars: 20 μm.

(D) Quantification of DDX6. Graph represents average ± SEM DDX6 intensity from n = 17–28 images/group; ****p < 0.0001.

(E) Representative histogram of Ki67 staining of primary human keratinocytes stimulated with vehicle control, 3 nM lfTSLP, or sfTSLP for 40 h. Isotype IgG used for control.

(F and G) Quantification of $Ki67^+$ (F) cell abundance and (G) Ki67 MFI in primary human keratinocytes stimulated with 3 nM lfTSLP and sfTSLP for 24 h. Data represent averages ± SEM of 3 independent experiments using 2 or 3 different human donors in technical triplicates. **p < 0.01, ***p < 0.001, and ****p < 0.0001.

See also Table S1.

changes in scratching behavior compared with vehicle-treated animals (data not shown). In contrast to our findings, s.c. injection of TSLP (2.5 μg, 10 times higher than the dose we used) into the cheek induced robust scratching behavior (Wilson et al., 2013). Thus, the observed phenotypic differences between our study and the earlier reports are likely due to differences in dose, timing, and location of TSLP delivery. One may predict that a short period of exposure of low-dose TSLP is beneficial under specific circumstances, such as hair growth, whereas

prolonged exposure of high-level TSLP induces skin and systemic atopic-like symptoms.

Recent studies have defined essential cues for hair cycle regulation that require heterologous cell populations and intricate crosstalk between stem cells and their progeny (Blanpain and Fuchs, 2014; Hsu and Fuchs, 2012; Hsu et al., 2011; Joost et al., 2018; Yang et al., 2017). TACs arise from the hair germ stem cells in response to cues from the underlying dermal papilla, which then confer signals to the bulge stem cells to complete hair growth (Greco et al., 2009; Hsu et al., 2011, 2014; Lien et al., 2011; Rompolas et al., 2013; Yang et al., 2017). We found that TSLP treatment drove the expansion of $CD34^{+}ITG\alpha6^{lo}$ cells, and this was correlated with keratinocyte TSLPR-dependent upregulation of cyclin D1. Additional studies will be required to dissect whether TSLP initiates activation of stem cells in the hair germ to initiate TAC expansion.

$CD34^{+}ITG\alpha6^{lo}$ and $CD34^{+}ITG\alpha6^{hi}$ cells are defined to retain multipotent function with capacity to regenerate epidermis, hair follicle, and sebaceous glands in mice (Blanpain et al., 2004; Morris et al., 2004). Interestingly, $CD34^{+}ITG\alpha6^{hi}CD200^{+}$ cells are lost in AGA patients, whereas $K15^{hi}ITG\alpha6^{hi}$ HFSCs are retained in the hair bulge, but they lack growth cues in AGA and are therefore unable to generate hair (Garza et al., 2011). TSLP was also found markedly reduced in patients with alopecia areata, and treatment with diphenylcyclopropenone elevated TSLP in patients that showed signs of hair growth (Gong et al., 2021). Microneedle treatments induce micro-injuries to activate hair cycling and constitute a common treatment of non-scarring alopecia types, achieving an impressive efficacy of more than 80% (Fertig et al., 2018; Hou et al., 2017). Our study provides functional insights for how wound-derived factors might drive hair growth. Additional studies are necessary to determine whether the findings obtained from animal model studies phenocopy human conditions and whether TSLP-TSLPR signaling can override signals inhibiting proliferation of HFSC in alopecia. Lasty, it will be interesting to see whether TSLP expression levels determine the probability of a patient's response to microneedle treatment.

In summary, this study demonstrates that TSLP promotes proliferation of HFSCs, driving wound-induced hair growth in mice. Further work is necessary to define the precise keratinocyte-intrinsic molecular mechanisms mediating TSLP/TSLPR signaling in HFSC. Additionally, it remains to be explored if and how TSLP modulates the immune microenvironment that may indirectly affect hair phenotypes. By identifying and dissecting the specific roles of TSLP in HFSCs and healing skin, our findings reveal a novel mechanism of hair growth and regeneration.

EXPERIMENTAL PROCEDURES

For further details, see supplemental experimental procedures.

Animal studies

C57BL6/J and $Lgr5^{CreER}$ (Jackson Laboratory, Bar Harbor, ME) and $Tslpr^{fl/fl}$ mice were maintained under specific pathogen-free conditions. Skin wounds (4 or 12 mm diameter) were induced on the back of anesthetized mice during 2nd telogen unless otherwise stated. Recombinant TSLP (555-TS-010; R&D Systems) (100 ng in 5 μL PBS) was delivered directly to the wound site immediately after wounding or delivered subcutaneously (250 ng in 100 μL 0.01% BSA in PBS) using a 31G needle. $Lgr5^{CreER}.Tslpr^{fl/fl}$ mice were treated with 50 μg 4-hydroxytamoxifen (H7904; Sigma-Aldrich) dissolved in 100% ethanol at postnatal day (p) 46, p48, and p50. 4OHT was delivered directly to the center back skin and wounds at p54.

SUPPLEMENTAL INFORMATION

Supplemental information can be found online at https://doi.org/10.1016/j.stemcr.2022.01.017.

AUTHOR CONTRIBUTIONS

J.L.S., J.Y.Z., and A.S.M. designed the studies. J.L.S. wrote the manuscript draft. J.L.S., J.Y.Z., and A.S.M. provided revisions. J.L.S. performed and designed the experiments and analyzed and interpreted the data. D.L.C. performed biocomputational data analyses. J.C.M. collected patient biopsy samples. J.Y.Z. and A.S.M. supervised the work and conceptualized and helped interpret the experimental results. S.F.Z. provided $Tslpr^{fl/fl}$ mice and insightful comments. All authors reviewed the manuscript.

CONFLICTS OF INTERESTS

A.S.M. consulted and received funds from Silab, but this funding was not directly used for this study. A.S.M. is currently employed by Janssen Pharmaceuticals. All other authors declare no competing interests.

ACKNOWLEDGMENTS

We would like to thank David Erdmann and Simone Degan (Duke University) for providing surgically discarded human skin tissues. We thank members of the Zhang lab for discussion. We thank Blanche Capel (Duke University) for help providing $Lgr5^{CreER}$ mice. We thank Dr. Maria Morasso (NIH) for sharing gene expression data. This work is in part supported by NIH/NIAID grant R01-AI139207 to A.S.M. and J.Y.Z., NIH/NIAMS grant R01-AR068991 to J.Y.Z., and the Department of Dermatology. A.S.M. was also supported by a Dermatology Foundation Award and Duke Physician-Scientist Strong Start Award.

Received: February 17, 2021
Revised: January 24, 2022
Accepted: January 25, 2022
Published: February 24, 2022

REFERENCES

Abbasi, S., and Biernaskie, J. (2019). Injury modifies the fate of hair follicle dermal stem cell progeny in a hair cycle-dependent manner. Exp. Dermatol. *28*, 419–424.

Abbasi, S., Sinha, S., Labit, E., Rosin, N.L., Yoon, G., Rahmani, W., Jaffer, A., Sharma, N., Hagner, A., Shah, P., et al. (2020). Distinct regulatory programs control the latent regenerative potential of dermal fibroblasts during wound healing. Cell Stem Cell *27*, 396–412.e6.

Al-Shami, A., Spolski, R., Kelly, J., Keane-Myers, A., and Leonard, W.J. (2005). A role for TSLP in the development of inflammation in an asthma model. J. Exp. Med. *202*, 829–839.

Allakhverdi, Z., Comeau, M.R., Jessup, H.K., Yoon, B.-R.P., Brewer, A., Chartier, S., Paquette, N., Ziegler, S.F., Sarfati, M., and Delespesse, G. (2007). Thymic stromal lymphopoietin is released by human epithelial cells in response to microbes, trauma, or inflammation and potently activates mast cells. J. Exp. Med. *204*, 253–258.

Barker, N., Bartfeld, S., and Clevers, H. (2010). Tissue-resident adult stem cell populations of rapidly self-renewing organs. Cell Stem Cell *7*, 656–670.

Bhoopalam, M., Garza, L.A., and Reddy, S.K. (2020). Wound induced hair neogenesis – a novel paradigm for studying regeneration and aging. Front. Cell Develop. Biol. *8*, 583446.

Bjerkan, L., Schreurs, O., Engen, S.A., Jahnsen, F.L., Baekkevold, E.S., Blix, I.J., and Schenck, K. (2015). The short form of TSLP is constitutively translated in human keratinocytes and has characteristics of an antimicrobial peptide. Mucosal Immunol. *8*, 49–56.

Blanpain, C., and Fuchs, E. (2014). Plasticity of epithelial stem cells in tissue regeneration. Science *344*, 1242281.

Blanpain, C., Lowry, W.E., Geoghegan, A., Polak, L., and Fuchs, E. (2004). Self-renewal, multipotency, and the existence of two cell populations within an epithelial stem cell niche. Cell *118*, 635–648.

Chase, H.B. (1954). Growth of the hair. Physiol. Rev. *34*, 113–126.

Chen, C.-C., Wang, L., Plikus, M.V., Jiang, .X., Murray, P.J., Ramos, R., Guerrero-Juarez, C.F., Hughes, M.W., Lee, O.K., Shi, S., et al. (2015). Organ-level quorum sensing directs regeneration in hair stem cell populations. Cell *161*, 277–290.

Chen, L., Arbieva, Z.H., Guo, S., Marucha, P.T., Mustoe, T.A., and DiPietro, L.A. (2010). Positional differences in the wound transcriptome of skin and oral mucosa. BMC Genomics *11*, 471.

Choa, R., Tohyama, J., Wada, S., Meng, H., Hu, J., Okumura, M., May, R.M., Robertson, T.F., Pai, R.L., Nace, A., et al. (2021). Thymic stromal lymphopoietin induces adipose loss through sebum hypersecretion. Science *373*, eabd2893.

Choi, Yeon S., Zhang, Y., Xu, M., Yang, Y., Ito, M., Peng, T., Cui, Z., Nagy, A., Hadjantonakis, A.-K., Lang, Richard A., et al. (2013). Distinct functions for Wnt/β-catenin in hair follicle stem cell proliferation and survival and interfollicular epidermal homeostasis. Cell Stem Cell *13*, 720–733.

Christmann, R.B., Mathes, A., Affandi, A.J., Padilla, C., Nazari, B., Bujor, A.M., Stifano, G., and Lafyatis, R. (2013). Thymic stromal lymphopoietin is up-regulated in the skin of patients with systemic sclerosis and induces profibrotic genes and intracellular signaling that overlap with those induced by interleukin-13 and transforming growth factor β. Arthritis Rheum. *65*, 1335–1346.

Corren, J., and Ziegler, S.F. (2019). TSLP: from allergy to cancer. Nat. Immunol. *20*, 1603–1609.

Cotsarelis, G., Sun, T.-T., and Lavker, R.M. (1990). Label-retaining cells reside in the bulge area of pilosebaceous unit: implications for follicular stem cells, hair cycle, and skin carcinogenesis. Cell *61*, 1329–1337.

Di Stefano, B., Luo, E.-C., Haggerty, C., Aigner, S., Charlton, J., Brumbaugh, J., Ji, F., Rabano Jiménez, I., Clowers, K.J., Huebner, A.J., et al. (2019). The RNA helicase DDX6 controls cellular plasticity by modulating P-body homeostasis. Cell Stem Cell *25*, 622–638.e3.

Fertig, R.M., Gamret, A.C., Cervantes, J., and Tosti, A. (2018). Microneedling for the treatment of hair loss? J. Eur. Acad. Dermatol. Venereol. *32*, 564–569.

Fornasa, G., Tsilingiri, K., Caprioli, F., Botti, F., Mapelli, M., Meller, S., Kislat, A., Homey, B., Di Sabatino, A., Sonzogni, A., et al. (2015). Dichotomy of short and long thymic stromal lymphopoietin isoforms in inflammatory disorders of the bowel and skin. J. Allergy Clin. Immunol. *136*, 413–422.

Ganti, K.P., Mukherji, A., Surjit, M., Li, M., and Chambon, P. (2017). Similarities and differences in the transcriptional control of expression of the mouse TSLP gene in skin epidermis and intestinal epithelium. Proc. Natl. Acad. Sci. U S A *114*, E951–E960.

Garza, L.A., Yang, C.-C., Zhao, T., Blatt, H.B., Lee, M., He, H., Stanton, D.C., Carrasco, L., Spiegel, J.H., Tobias, J.W., et al. (2011). Bald scalp in men with androgenetic alopecia retains hair follicle stem cells but lacks CD200-rich and CD34-positive hair follicle progenitor cells. J. Clin. Invest. *121*, 613–622.

Gay, D., Kwon, O., Zhang, Z., Spata, M., Plikus, M.V., Holler, P.D., Ito, M., Yang, Z., Treffeisen, E., Kim, C.D., et al. (2013). Fgf9 from dermal γδ T cells induces hair follicle neogenesis after wounding. Nat. Med. *19*, 916–923.

Ge, Y., Gomez, N.C., Adam, R.C., Nikolova, M., Yang, H., Verma, A., Lu, C.P.-J., Polak, L., Yuan, S., Elemento, O., et al. (2017). Stem cell lineage infidelity drives wound repair and cancer. Cell *169*, 636–650.e4.

Gong, Y., Luo, L., Li, L., He, X., Lu, W., Sha, X., and Mao, Y. (2021). Diphenylcyclopropenone plays an effective therapeutic role by up-regulating the TSLP/OX40L/IL-13 pathway in severe alopecia areata. Exp. Dermatol. *30*, 278–283.

Greco, V., Chen, T., Rendl, M., Schober, M., Pasolli, H.A., Stokes, N., dela Cruz-Racelis, J., and Fuchs, E. (2009). A two-step mechanism for stem cell activation during hair regeneration. Cell Stem Cell *4*, 155–169.

Handjiski, B.K., EichmÜLler, S., Hofmann, U., Czarnetzki, B.M., and Paus, R. (1994). Alkaline phosphatase activity and localization during the murine hair cycle. Br. J. Dermatol. *131*, 303–310.

He, R., Oyoshi, M.K., Garibyan, L., Kumar, L., Ziegler, S.F., and Geha, R.S. (2008). TSLP acts on infiltrating effector T cells to drive allergic skin inflammation. Proc. Natl. Acad. Sci. U S A *105*, 11875.

Hou, A., Cohen, B., Haimovic, A., and Elbuluk, N. (2017). Microneedling: a comprehensive review. Dermatol. Surg. *43*, 321–339.

Hsu, Y.-C., and Fuchs, E. (2012). A family business: stem cell progeny join the niche to regulate homeostasis. Nat. Rev. Mol. Cell Biol. *13*, 103–114.

Hsu, Y.-C., Li, L., and Fuchs, E. (2014). Transit-amplifying cells orchestrate stem cell activity and tissue regeneration. Cell *157*, 935–949.

Hsu, Y.-C., Pasolli, H.A., and Fuchs, E. (2011). Dynamics between stem cells, niche, and progeny in the hair follicle. Cell *144*, 92–105.

Hunt, N., and McHale, S. (2005). The psychological impact of alopecia. BMJ *331*, 951–953.

Iglesias-Bartolome, R., Uchiyama, A., Molinolo, A.A., Abusleme, L., Brooks, S.R., Callejas-Valera, J.L., Edwards, D., Doci, C., Asselin-Labat, M.-L., Onaitis, M.W., et al. (2018). Transcriptional signature primes human oral mucosa for rapid wound healing. Sci. Transl. Med. *10*, eaap8798.

Imai, Y. (2019). Interleukin-33 in atopic dermatitis. J. Dermatol. Sci. *96*, 2–7.

Islam, S.A., and Luster, A.D. (2012). T cell homing to epithelial barriers in allergic disease. Nat. Med. *18*, 705–715.

Ito, M., Liu, Y., Yang, Z., Nguyen, J., Liang, F., Morris, R.J., and Cotsarelis, G. (2005). Stem cells in the hair follicle bulge contribute to wound repair but not to homeostasis of the epidermis. Nat. Med. *11*, 1351–1354.

Ito, M., Yang, Z., Andl, T., Cui, C., Kim, N., Millar, S.E., and Cotsarelis, G. (2007). Wnt-dependent de novo hair follicle regeneration in adult mouse skin after wounding. Nature *447*, 316–320.

Jaks, V., Barker, N., Kasper, M., van Es, J.H., Snippert, H.J., Clevers, H., and Toftgård, R. (2008). Lgr5 marks cycling, yet long-lived, hair follicle stem cells. Nat. Genet. *40*, 1291–1299.

Jensen, U.B., Yan, X., Triel, C., Woo, S.-H., Christensen, R., and Owens, D.M. (2008). A distinct population of clonogenic and multipotent murine follicular keratinocytes residing in the upper isthmus. J. Cell Sci. *121*, 609.

Joost, S., Jacob, T., Sun, X., Annusver, K., La Manno, G., Sur, I., and Kasper, M. (2018). Single-cell transcriptomics of traced epidermal and hair follicle stem cells reveals rapid adaptations during wound healing. Cell Rep. *25*, 585–597.e7.

Kabata, H., Flamar, A.-L., Mahlakõiv, T., Moriyama, S., Rodewald, H.-R., Ziegler, S.F., and Artis, D. (2020). Targeted deletion of the TSLP receptor reveals cellular mechanisms that promote type 2 airway inflammation. Mucosal Immunol. *13*, 626–636.

Kato, A., Favoreto, S., Jr., Avila, P.C., and Schleimer, R.P. (2007). TLR3- and Th2 cytokine-dependent production of thymic stromal lymphopoietin in human airway epithelial cells. J. Immunol. *179*, 1080–1087.

Kim, B.S., Siracusa, M.C., Saenz, S.A., Noti, M., Monticelli, L.A., Sonnenberg, G.F., Hepworth, M.R., Van Voorhees, A.S., Comeau, M.R., and Artis, D. (2013). TSLP elicits IL-33–independent innate lymphoid cell responses to promote skin inflammation. Sci. Transl. Med. *5*, 170ra116.

Kim, D., Chen, R., Sheu, M., Kim, N., Kim, S., Islam, N., Wier, E.M., Wang, G., Li, A., Park, A., et al. (2019). Noncoding dsRNA induces retinoic acid synthesis to stimulate hair follicle regeneration via TLR3. Nat. Commun. *10*, 2811.

Kim, D., Hossain, M.Z., Nieves, A., Gu, L., Ratliff, T.S., Mi Oh, S., Park, A., Han, S., Yang, N.B., Qi, J., et al. (2016). To control site-specific skin gene expression, autocrine mimics paracrine canonical Wnt signaling and is activated ectopically in skin disease. Am. J. Pathol. *186*, 1140–1150.

Kubo, T., Kamekura, R., Kumagai, A., Kawata, K., Yamashita, K., Mitsuhashi, Y., Kojima, T., Sugimoto, K., Yoneta, A., Sumikawa, Y., et al. (2014). ΔNp63 controls a TLR3-mediated mechanism that abundantly provides thymic stromal lymphopoietin in atopic dermatitis. PLoS One *9*, e105498.

Leichner, T.M., Satake, A., Harrison, V.S., Tanaka, Y., Archambault, A.S., Kim, B.S., Siracusa, M.C., Leonard, W.J., Naji, A., Wu, G.F., et al. (2017). Skin-derived TSLP systemically expands regulatory T cells. J. Autoimmun. *79*, 39–52.

Levy, V., Lindon, C., Zheng, Y., Harfe, B.D., and Morgan, B.A. (2007). Epidermal stem cells arise from the hair follicle after wounding. FASEB J. *21*, 1358–1366.

Leyva-Castillo, J.M., Hener, P., Michea, P., Karasuyama, H., Chan, S., Soumelis, V., and Li, M. (2013). Skin thymic stromal lymphopoietin initiates Th2 responses through an orchestrated immune cascade. Nat. Commun. *4*, 2847.

Li, M., Messaddeq, N., Teletin, M., Pasquali, J.-L., Metzger, D., and Chambon, P. (2005). Retinoid X receptor ablation in adult mouse keratinocytes generates an atopic dermatitis triggered by thymic stromal lymphopoietin. Proc. Natl. Acad. Sci. U S A *102*, 14795–14800.

Lien, W.H., Guo, X., Polak, L., Lawton, L.N., Young, R.A., Zheng, D., and Fuchs, E. (2011). Genome-wide maps of histone modifications unwind in vivo chromatin states of the hair follicle lineage. Cell Stem Cell *9*, 219–232.

Lim, C.H., Sun, Q., Ratti, K., Lee, S.-H., Zheng, Y., Takeo, M., Lee, W., Rabbani, P., Plikus, M.V., Cain, J.E., et al. (2018). Hedgehog stimulates hair follicle neogenesis by creating inductive dermis during murine skin wound healing. Nat. Commun. *9*, 4903.

Morris, R.J., Liu, Y., Marles, L., Yang, Z., Trempus, C., Li, S., Lin, J.S., Sawicki, J.A., and Cotsarelis, G. (2004). Capturing and profiling adult hair follicle stem cells. Nat. Biotechnol. *22*, 411–417.

Müller-Röver, S., Foitzik, K., Paus, R., Handjiski, B., van der Veen, C., Eichmüller, S., McKay, I.A., and Stenn, K.S. (2001). A comprehensive guide for the accurate classification of murine hair follicles in distinct hair cycle stages. J. Invest. Dermatol. *117*, 3–15.

Nelson, A.M., Loy, D.E., Lawson, J.A., Katseff, A.S., FitzGerald, G.A., and Garza, L.A. (2013). Prostaglandin D_2 inhibits wound-induced hair follicle neogenesis through the receptor, Gpr44. J. Invest. Dermatol. *133*, 881–889.

Nelson, A.M., Reddy, S.K., Ratliff, T.S., Hossain, M.Z., Katseff, A.S., Zhu, A.S., Chang, E., Resnik, S.R., Page, C., Kim, D., et al. (2015). dsRNA released by tissue damage activates TLR3 to drive skin regeneration. Cell Stem Cell *17*, 139–151.

Ostareck, D.H., Naarmann-de Vries, I.S., and Ostareck-Lederer, A. (2014). DDX6 and its orthologs as modulators of cellular and viral RNA expression. WIRE RNA *5*, 659–678.

Oyoshi, M.K., Larson, R.P., Ziegler, S.F., and Geha, R.S. (2010). Mechanical injury polarizes skin dendritic cells to elicit a T(H)2

response by inducing cutaneous thymic stromal lymphopoietin expression. J. Allergy Clin. Immunol. *126*, 976–984.e5.

Pandey, A., Ozaki, K., Baumann, H., Levin, S.D., Puel, A., Farr, A.G., Ziegler, S.F., Leonard, W.J., and Lodish, H.F. (2000). Cloning of a receptor subunit required for signaling by thymic stromal lymphopoietin. Nat. Immunol. *1*, 59–64.

Rahmani, W., Liu, Y., Rosin, N.L., Kline, A., Raharjo, E., Yoon, J., Stratton, J.A., Sinha, S., and Biernaskie, J. (2018). Macrophages promote wound-induced hair follicle regeneration in a CX_3CR1- and TGF-β1–dependent manner. J. Invest. Dermatol. *138*, 2111–2122.

Reche, P.A., Soumelis, V., Gorman, D.M., Clifford, T., Liu, M., Travis, M., Zurawski, S.M., Johnston, J., Liu, Y.J., Spits, H., et al. (2001). Human thymic stromal lymphopoietin preferentially stimulates myeloid cells. J. Immunol. *167*, 336–343.

Rochman, Y., and Leonard, W.J. (2008). The role of thymic stromal lymphopoietin in $CD8^+$ T cell homeostasis. J. Immunol. *181*, 7699.

Rompolas, P., Mesa, K.R., and Greco, V. (2013). Spatial organization within a niche as a determinant of stem-cell fate. Nature *502*, 513–518.

Saed, S., Ibrahim, O., and Bergfeld, W.F. (2017). Hair camouflage: a comprehensive review. Int. J. Womens Dermatol. *3*, S75–S80.

Salimi, M., Barlow, J.L., Saunders, S.P., Xue, L., Gutowska-Owsiak, D., Wang, X., Huang, L.-C., Johnson, D., Scanlon, S.T., McKenzie, A.N.J., et al. (2013). A role for IL-25 and IL-33–driven type-2 innate lymphoid cells in atopic dermatitis. J. Exp. Med. *210*, 2939–2950.

Shane, H.L., and Klonowski, K.D. (2014). A direct and nonredundant role for thymic stromal lymphopoietin on antiviral CD8 T cell responses in the respiratory mucosa. J. Immunol. *192*, 2261–2270.

Snippert, H.J., Haegebarth, A., Kasper, M., Jaks, V., van Es, J.H., Barker, N., van de Wetering, M., van den Born, M., Begthel, H., Vries, R.G., et al. (2010). Lgr6 marks stem cells in the hair follicle that generate all cell lineages of the skin. Science *327*, 1385.

Stenn, K.S., and Paus, R. (2001). Controls of hair follicle cycling. Physiol. Rev. *81*, 449–494.

Tanaka, J., Watanabe, N., Kido, M., Saga, K., Akamatsu, T., Nishio, A., and Chiba, T. (2009). Human TSLP and TLR3 ligands promote differentiation of Th17 cells with a central memory phenotype under Th2-polarizing conditions. Clin. Exp. Allergy *39*, 89–100.

Tao, Y., Wang, Y., Wang, X., Wang, C., Bao, K., Ji, L., Jiang, G., and Hong, M. (2017). Calycosin suppresses epithelial derived initiative key factors and maintains epithelial barrier in allergic inflammation via TLR4 mediated NF-κB pathway. Cell Physiol. Biochem. *44*, 1106–1119.

Tetsu, O., and McCormick, F. (1999). β-Catenin regulates expression of cyclin D1 in colon carcinoma cells. Nature *398*, 422–426.

Verstraete, K., Peelman, F., Braun, H., Lopez, J., Van Rompaey, D., Dansercoer, A., Vandenberghe, I., Pauwels, K., Tavernier, J., Lambrecht, B.N., et al. (2017). Structure and antagonism of the receptor complex mediated by human TSLP in allergy and asthma. Nat. Commun. *8*, 14937.

Wang, X., Chen, H., Tian, R., Zhang, Y., Drutskaya, M.S., Wang, C., Ge, J., Fan, Z., Kong, D., Wang, X., et al. (2017). Macrophages induce AKT/β-catenin-dependent Lgr5+ stem cell activation and hair follicle regeneration through TNF. Nat. Commun. *8*, 14091.

Wang, Y., Arribas-Layton, M., Chen, Y., Lykke-Andersen, J., and Sen, G.L. (2015). DDX6 orchestrates mammalian progenitor function through the mRNA degradation and translation pathways. Mol. Cell *60*, 118–130.

Wier, E.M., and Garza, L.A. (2020). Through the lens of hair follicle neogenesis, a new focus on mechanisms of skin regeneration after wounding. Semin. Cell Develop. Biol. *100*, 122–129.

Wilson, S.R., Thé, L., Batia, L.M., Beattie, K., Katibah, G.E., McClain, S.P., Pellegrino, M., Estandian, D.M., and Bautista, D.M. (2013). The epithelial cell-derived atopic dermatitis cytokine TSLP activates neurons to induce itch. Cell *155*, 285–295.

Yang, H., Adam, R.C., Ge, Y., Hua, Z.L., and Fuchs, E. (2017). Epithelial-mesenchymal micro-niches govern stem cell lineage choices. Cell *169*, 483–496.e3.

Stem Cell Reports, Volume *17*

Supplemental Information

Thymic stromal lymphopoietin controls hair growth

Jessica L. Shannon, David L. Corcoran, John C. Murray, Steven F. Ziegler, Amanda S. MacLeod, and Jennifer Y. Zhang

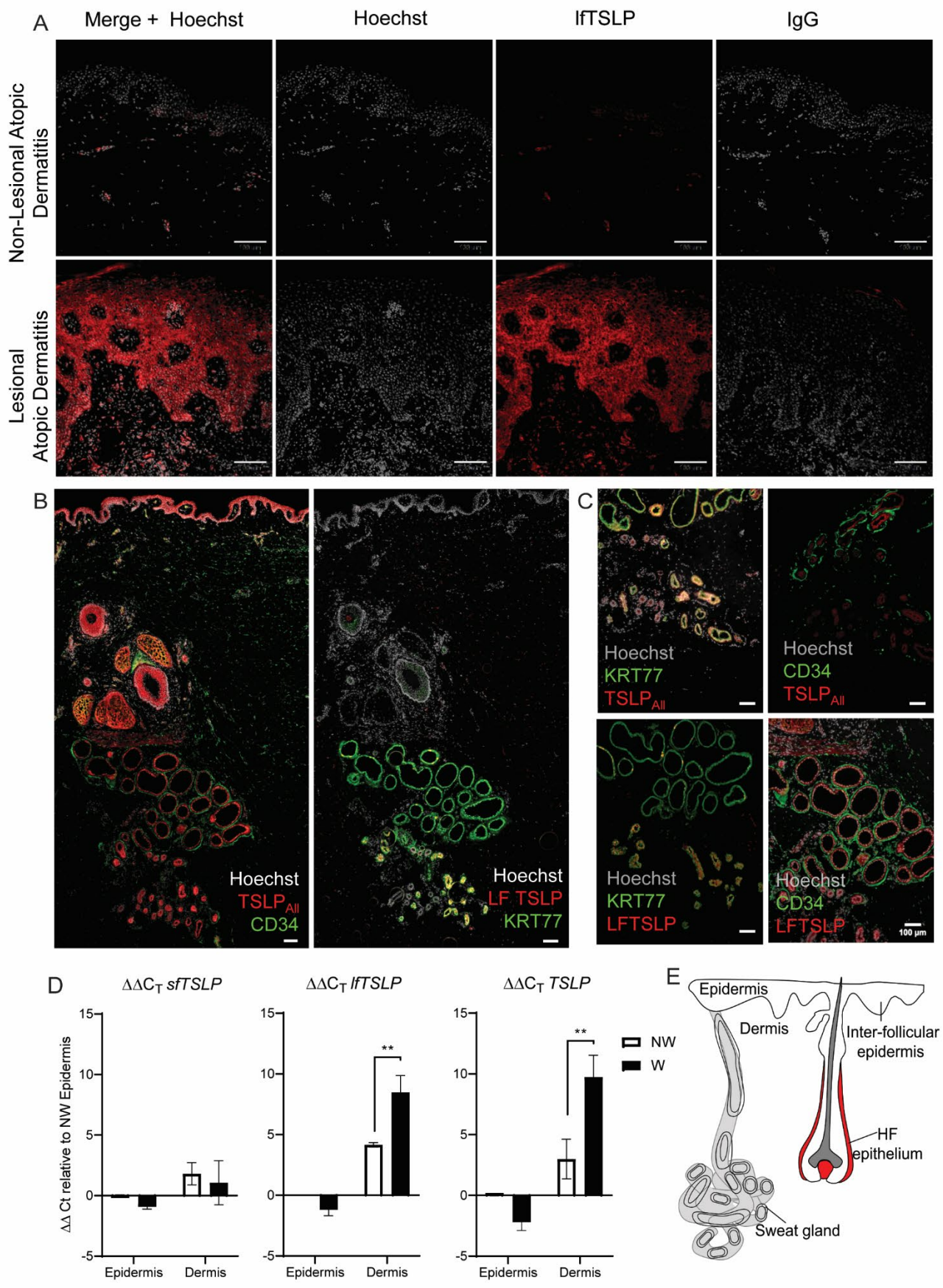
A
Merge + Hoechst
Hoechst
lfTSLP
IgG
Non-Lesional Atopic Dermatitis
Lesional Atopic Dermatitis
B
Hoechst
TSLP All
CD34
Hoechst
LF TSLP
KRT77
C
Hoechst
KRT77
TSLP All
Hoechst
CD34
TSLP All
Hoechst
KRT77
LFTSLP
Hoechst
CD34
LFTSLP
100 µm
D
ΔΔC T sfTSLP
ΔΔC T lfTSLP
ΔΔC T TSLP
ΔΔ Ct relative to NW Epidermis
15
10
5
0
-5
**
Epidermis
Dermis
NW
W
E
Epidermis
Dermis
Inter-follicular epidermis
HF epithelium
Sweat gland

Figure S1: Human lfTSLP is expressed in glandular structures in the dermis. *Related to Figure 1.*

A. Immunostaining lfTSLP in lesional and non-lesional tissue samples collected from atopic dermatitis patients. Scale = 100 μm**.**

B-C. Representative immunostaining of human skin of $TSLP_{total}$ or long form TSLP (red) and CD34 or KRT77 (green) Data presented are from n=3 independent experiments using 3 different human donors. Scale bar = 100 μm**.**

D. qPCR showing $\Delta\Delta C_T$ value for gene expression of each *TSLP* isoform from epidermis or dermis in response to 24h wound *ex vivo*. Values are normalized to NW epidermis for this tissue sample. Data presented are from n=4 independent experiments using 2 different human donors in technical duplicate. Error bars represent ± SEM.

E. Schematic illustration representing cross section of human skin with sweat gland and hair follicle residing in dermis.

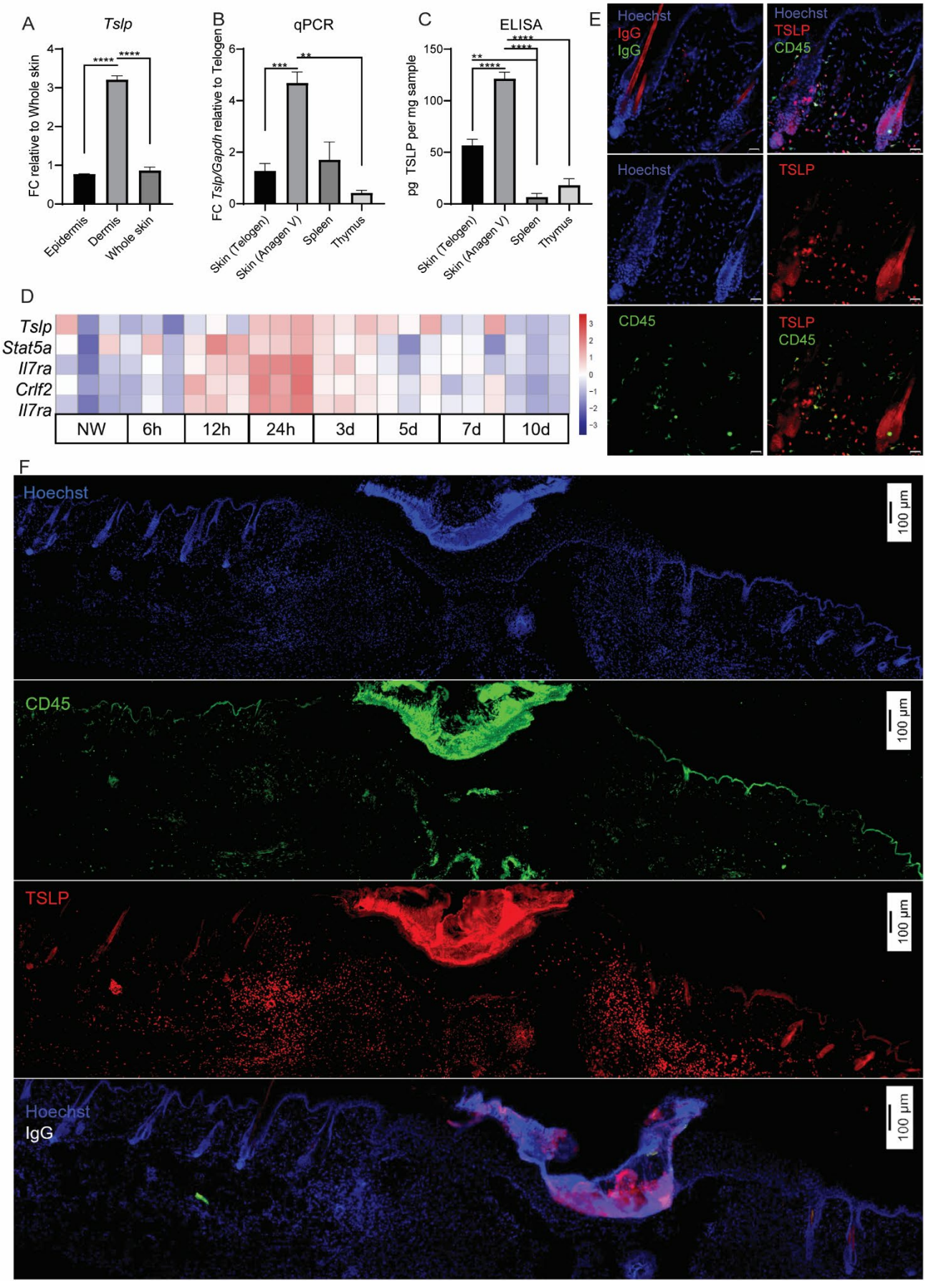
A
Tslp
FC relative to Whole skin
Epidermis
Dermis
Whole skin
B
qPCR
FC Tslp/Gapdh relative to Telogen
Skin (Telogen)
Skin (Anagen V)
Spleen
Thymus
C
ELISA
pg TSLP per mg sample
D
Tslp
Stat5a
Il7ra
Crlf2
Il7ra
NW
6h
12h
24h
3d
5d
7d
10d
E
Hoechst
IgG
IgG
Hoechst
TSLP
CD45
Hoechst
TSLP
CD45
TSLP
CD45
F
Hoechst
CD45
TSLP
Hoechst
IgG
100 µm

Figure S2: TSLP is expressed in mouse skin after wounding. *Related to Figure 1*

A. qPCR for *Tslp* from epidermis or dermis isolated from healthy, non-wounded mouse back skin; data are normalized to *Tslp* expression from whole skin.

B-C. Gene expression TSLP by qPCR (**B**) or ELISA (**C**) from skin and lymphoid organs. Statistics by one-way ANOVA where n=3 mice (thymus); n=3 mice (spleen); n=11 mice (telogen skin); n=31 mice (Anagen V) for qPCR and n=3 mice (thymus); n=4 mice (spleen); n=19 mice (telogen skin); n=13 mice (Anagen V) for ELISA.

D. Heatmap representation of gene expression of healing excisional wounds in balb/c mice (GSE23006). The normalized expression data has been z-score transformed for each gene across the time-course.

E-F. Immunostaining of skin samples collected 7d after wounding. Scale bar: 20 μm (E) and 100 μm (F).

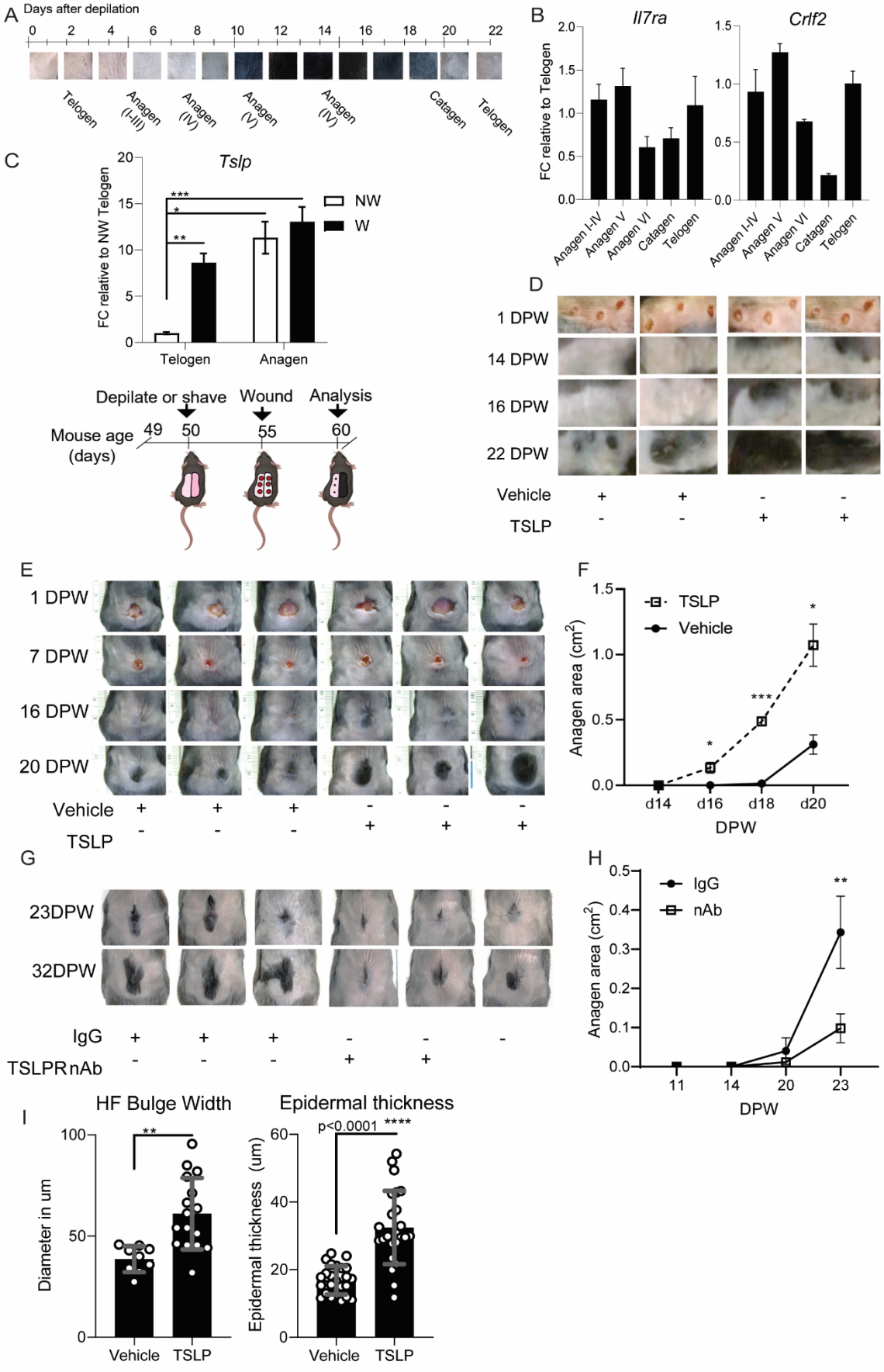
A
Days after depilation
0 2 4 6 8 10 12 14 16 18 20 22
Telogen
Anagen (I-III)
Anagen (IV)
Anagen (V)
Anagen (VI)
Catagen
Telogen
B
Il7ra
Crlf2
FC relative to Telogen
Anagen I-IV
Anagen V
Anagen VI
Catagen
Telogen
C
Tslp
FC relative to NW Telogen
NW
W
Telogen
Anagen
Depilate or shave
Wound
Analysis
Mouse age (days)
49
50
55
60
D
1 DPW
14 DPW
16 DPW
22 DPW
Vehicle
TSLP
E
1 DPW
7 DPW
16 DPW
20 DPW
Vehicle
TSLP
F
TSLP
Vehicle
Anagen area (cm2)
d14
d16
d18
d20
DPW
G
23DPW
32DPW
IgG
TSLPR nAb
H
IgG
nAb
Anagen area (cm2)
11
14
20
23
DPW
I
HF Bulge Width
Diameter in um
Vehicle
TSLP
Epidermal thickness
p<0.0001 ****
Epidermal thickness (um)
Vehicle
TSLP

Figure S3: TSLP accelerates WIHG. *Related to Figure 2.*

A. Photos of mouse skin during active hair cycling showing changes in skin pigment in C57BL/6 mice.

B. qPCR of gene expression of *Il7r* and *Crlf2* in whole skin in each hair follicle stage. Data presented are from n=2 experiments using n=27 mice (anagen I-IV); n=8 mice (anagen V); n=9 mice (anagen VI); n=3 mice (catagen); n=3 mice(telogen).

C. qPCR analysis of *Tslp* from wounded or non-wounded back skin (5dpw). Hair cycles of mice were synchronized, and wounds were induced during telogen or anagen (5 days after depilation) with timeline (right). Data presented are from n=1 experiment using n=3 mice per group.

D. Representative photographs of healing mouse wounds (4-mm full thickness wounds) after treatment with TSLP (100ng/wound) or vehicle.

E-F. Photographs of healing mouse wounds (E) and quantification (F) of total skin area that has entered anagen during WIHN assay (wound area=1.2 cm^2) treated with mTslp (250ng total) or vehicle (0.1%BSA) on the day of wounding. Data presented are from n=2 experiments using n=4-6 mice per group.

G-H. Photographs (G) and quantification of skin in anagen (H) from mice after WIHN assay (wound area=1.2 cm^2) treated with TSLPR neutralizing antibody (1ug total) or Rat IgG2A (1ug) on the day of wounding and 4 days after wounding. Photographs are representative of 4 mice per group across 1 experiment on 23DPW and 32DPW. nAb, neutralizing TSLPR antibody. IgG, Immunoglobulin. control.

I. Measurements of hair follicle at widest point (left) and epidermal thickness (right) from mouse skin 13 days after treatment with vehicle or TSLP Data presented are from n=2 experiments using n=3 mice per group and 11-30 unique sections of tissue were analyzed.

Statistics determined using t-test where $p<0.01$ **, $p<0.0001$**** Error bars represent ± SEM.

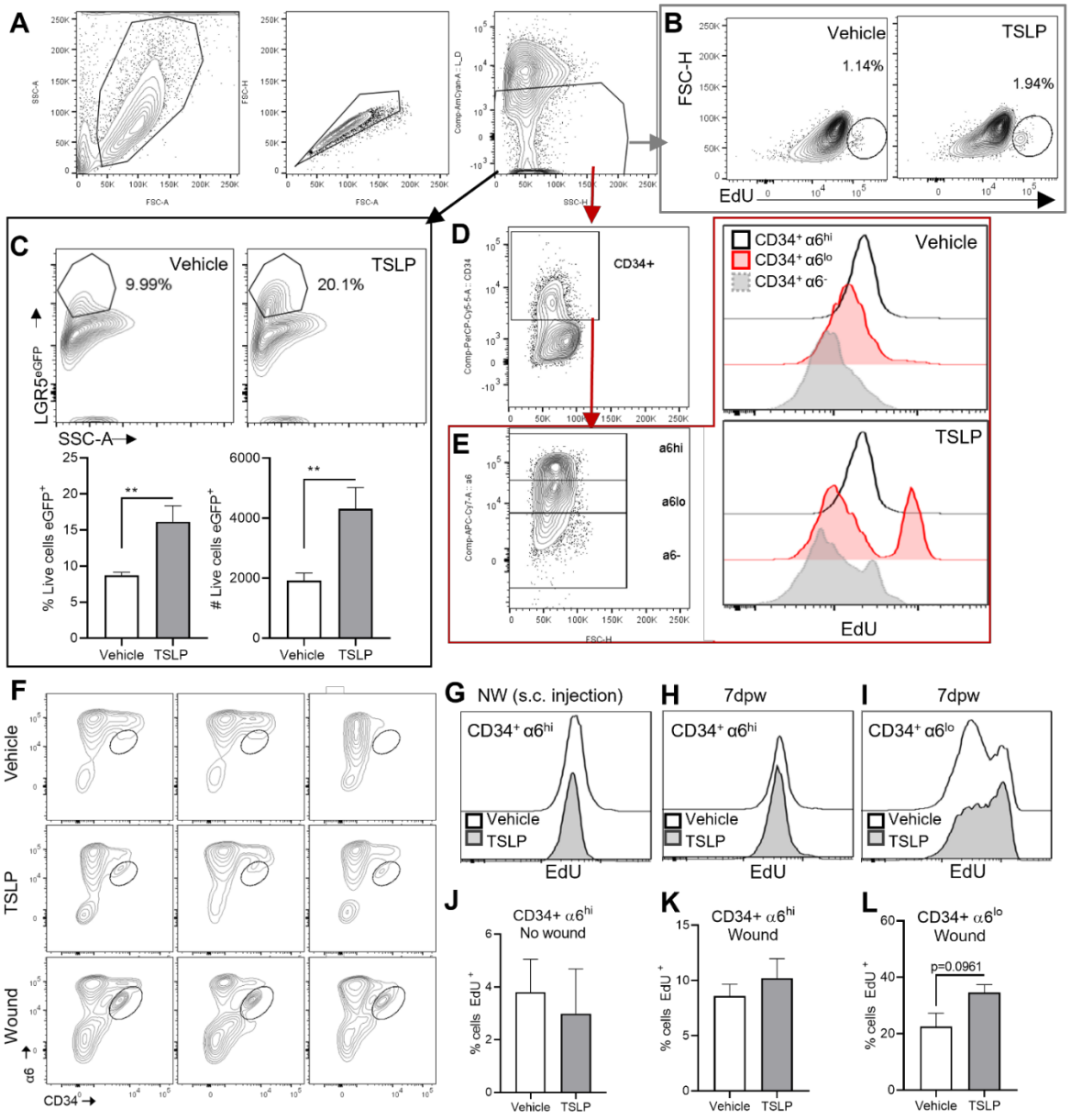

Figure S4: TSLP promotes proliferation of transit amplifying cells. *Related to Figure 3.*

A. Gating strategy for flow cytometry to live, single cells for analysis.

B. Flow cytometry plots showing total EdU+ cells pregated on live, single cells.

C. Quantification of LGR5+ HFSC after 7d s.c. TSLP treatment by flow cytometry from *Lgr5*^{CreER} transgenic mice. Data representative of n=4 mice across 2 experiments**.**

D-E. Gating strategy for flow cytometry to CD34+ cells (D), α6 subsets and histogram showing EdU expression for each α6 subset (E).

F. Flow cytometry plots showing a6 and CD34 expression, gated on live cells.

G-L. Histogram (G-I) and quantification (J-L) of EdU expression for CD34^{+} α6^{hi} and CD34^{+} α6^{lo} cells isolated from mice treated with TSLP or vehicle control for 7 days (G, J) or wounded and treated with vehicle or TSLP for 7 days (H, K). Data presented are representative of n=4 mice across 2 experiments.

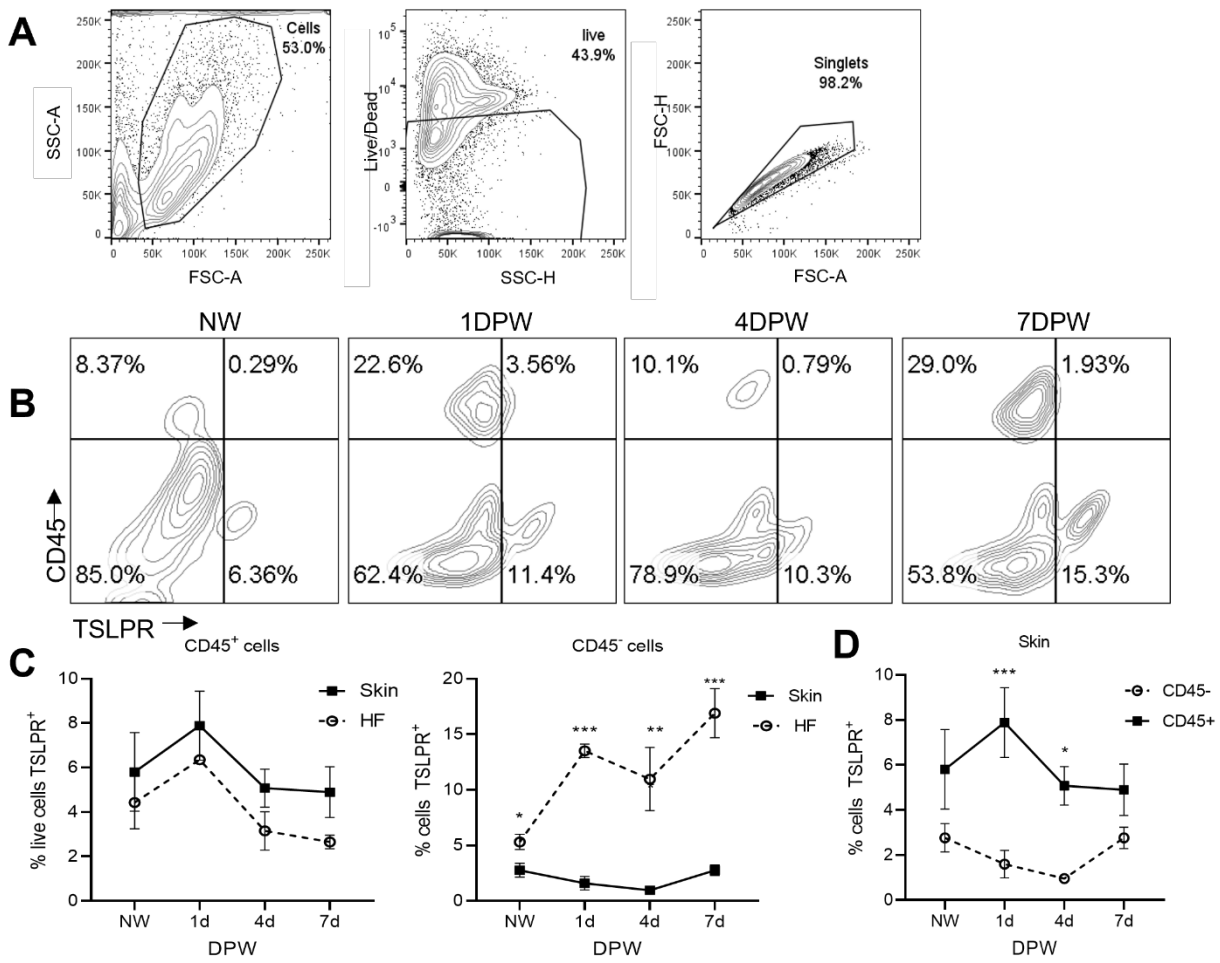

Figure S5: TSLPR expression is enriched in HF epithelial cells. *Related to Figure 4.*

A. Gating strategy for flow cytometry to live, single cells for analysis.

B. Flow plots for total live cells isolated from hair follicles during wound healing.

C. Quantification of TSLPR+ cells from HF or skin separated by CD45 antigen Data presented are from n=2 independent experiments using n=2-4 mice per group in technical duplicate.

D. Flow cytometry for TSLPR^{+} cells between 0 and 7dpw isolated from skin after wounding. Data presented are from n=2 independent experiments using n=2-4 mice per group in technical duplicate.

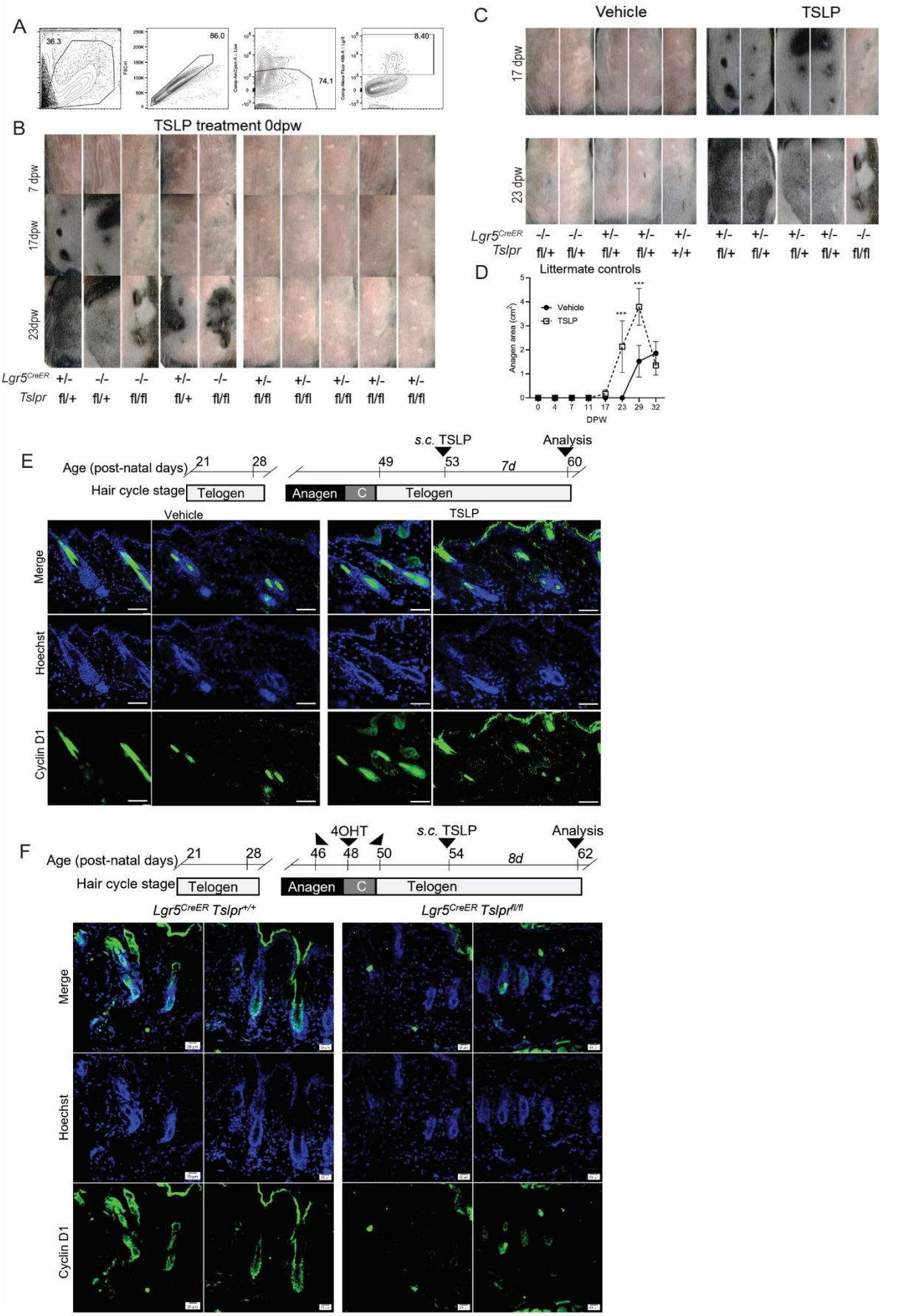
A
36.3
86.0
74.1
8.40
B
TSLP treatment 0dpw
7 dpw
17dpw
23dpw
Lgr5CreER +/- -/- -/- +/- -/- +/- +/- +/- +/- +/-
Tslpr fl/+ fl/+ fl/fl fl/+ fl/fl fl/fl fl/fl fl/fl fl/fl fl/fl
C
Vehicle
TSLP
17 dpw
23 dpw
Lgr5CreER -/- -/- +/- +/- +/- +/- +/- +/- +/- -/-
Tslpr fl/+ fl/+ fl/+ fl/+ +/+ fl/+ fl/+ fl/+ fl/+ fl/fl
D
Littermate controls
Vehicle
TSLP
Anagen area (cm2)
DPW
0 4 7 11 17 23 29 32
E
s.c. TSLP
Analysis
Age (post-natal days) 21 28 49 53 7d 60
Hair cycle stage Telogen Anagen C Telogen
Vehicle
TSLP
Merge
Hoechst
Cyclin D1
F
4OHT
s.c. TSLP
Analysis
Age (post-natal days) 21 28 46 48 50 54 8d 62
Hair cycle stage Telogen Anagen C Telogen
Lgr5CreER Tslpr+/+
Lgr5CreER Tslprfl/fl
Merge
Hoechst
Cyclin D1

Figure S6: TSLPR expression in keratinocyte is essential for WHIG. *Related to Figure 5.*

A. Gating strategy for flow cytometry to live, single, CD34+ cells for analysis in Figure 5.

B. Photographs of *Lgr5^{CreER}.Tslpr$^{fl/fl}$* mice, *Lgr5^{CreER}.Tslpr$^{fl/+}$* mice, and *Tslpr$^{fl/fl}$* mice treated with 4-hydroxytamoxifen (4OHT) prior to excisional wound and TSLP treatment.

C-D. Photographs (C) and quantification WIHG (D) of *Lgr5^{CreER}.Tslpr$^{fl/fl}$* mice, *Lgr5^{CreER}.Tslpr$^{fl/+}$* mice treated with TSLP or vehicle on day 0 after wounding. All mice were treated with 4OHT prior to wound. Data are representative of n=4 mice across 3 experiments.

E. Timeline and immunostaining for Cyclin D1 (green) in wild-type mice treated with *s.c*. Vehicle or TSLP. Scale: 50 μm.

F. Timeline and immunostaining for Cyclin D1 (green) in *Lgr5^{CreER}.Tslpr$^{fl/fl}$* or littermate control mice treated with 4OHT preceding *s.c*. injection with Vehicle or TSLP for 7 days. Scale: 20 μm.

Table S1: Gene expression analysis comparing healing skin wounds to TSLP-treated skin.
Upregualted genes collected during transition from inflammatory to proliferative phase of healing wounds in mouse or human skin that overlap with genes upregulated following subcutaneous TSLP treatment**.**
Related to Figure 6.

Compare to mouse skin 24h wound vs control (GSE23006)	Compare to human day6 vs day1 wound (control) (GSE97615)	Overlapping Mouse and Human Genes
Ccl5	*CSF3*	*DDX6*
Csf3	*IL1rl1*	*STAT1*
Il1rl1	*CXCL11*	*CXCL5*
Cxcl11	*GRB14*	*TLR2*
Gdap10	*IL6*	*PTGS2*
Saa3	*CXCL2*	*CD274*
Il6	*FABP4*	*MMP3*
Iigp1	*MMP3*	*CXCL2*
Cxcl2	*TNFRSF9*	*IL6*
Gbp2	*CXCL11*	*CXCL11*
Gbp2b	*CD274*	*IL1RL1*
Mmp3	*PTGS2*	*CSF3*
Clec4d	*TLR2*	
Cxcl1	*STEAP1*	
Cd274	*GSMB*	
Ddx6	*SLAMF7*	
Cxcl1	*CTLA4*	
Car4	*CXCL5*	
Irgm2	*CXCL17*	
Ptgs2	*CXCL9*	
Tlr2	*STAT1*	
Gbp3	*GBP6*	
Ifit2	*DDX6*	
Cxcl5		
Stat1		

Table S2: Primers used for qPCR.

Species and Gene	**Forward (5'-3')**	**Reverse (3'-5')**
Mouse *Tslp*	TTTGCCCGGAGAACAAGAG	TTTGGACTTCTTGTGCCATTTC
Human *TSLPtotal*	TTTGGAGATAGGCAGCTTCAG	AGGTGTGAGGAAAGTTCAAGAG
Human *lfTSLP*	GACTGGCAATGAGAGGCAAA	TCTTCCCACCACGAGTGTAA
Human *sfTSLP*	CGTAAACTTTGCCGCCTATGA	ACTCGGTACTTTTGGTCCCACTCA
Human *FLG*	GGTAGGTTAAGACATGAAGGATTTGC	GCTTGAGCCAACTTGAATACCAT
Mouse *Crlf2*	CTACATGACCCTGTGACCTTG	GGCACAGGATTTGTGAGTTTG
Mouse *Il7r*	GCGTATGTCACCATGTCTAGTT	AGCATTCCAGACTTTCCATCTC
Human *GAPDH*	ATGGGAAGGTGAAGGTCGGA	CAGCGTCAAAGGTGGAGGAGT5
Mouse *Gapdh*	GCACAGTCAAGGCCGAGAAT AGGTCGGTGTGAACGGATTTG	GCCTTCTCCATGGTGGTGAA TGTAGACCATGTAGTTGAGGTCA
Human *DDX6*	AGCCCGAGGAATCAACAATAG	ACTGGGTAGAAAGGGAAGAGA

Table S3: Primers used for Genotyping.

Primers used for mouse Genotyping		
Mouse *Tslpr*^{flox}	GGAGAGCAATGACGATGAGG	GAACCCGGAAGTCATAGCAG
Mouse *Lgr5*^{CreERT2}	CCTACTCGAAGACTTACCCAGT	GCATTGGGGTGAATGATAGCA

Table S4: STAR Methods reagent and resource table

REAGENT or RESOURCE	SOURCE	IDENTIFIER
Antibodies		
Mouse TSLPR-APC (Clone 22H9)	Biolegend	151805
Mouse TSLPR-BV421(Clone 22H9)	Biolegend	151807
Mouse CD45-Pacific Blue (Clone 30-F11)	Biolegend	103126
Mouse CD3-PE (Clone 17A2)	Tonbo	50-0032-U100
Mouse TSLP (Clone 17A2)	Biolegend	515202
Mouse CD34-PE (Clone Mec14.7)	Biolegend	119307
Mouse CD49f-AF647 (GoH3)	Biolegend	313610
antiEGFP-Af488 (pAb)	Invitrogen	A-21311
Mouse CD31-APC (Clone 390)	Biolegend	102410
Mouse Thy1.2-PerCP-Cy5.5 (Clone 53-21)	Biolegend	140322
Mouse Ki67 (Clone SP6)	Invitrogen	MA5-14520
Mouse TSLP nAb (Clone 152614)	Novus Bio	MAB555100
Human TSLP	Abcam	Ab47943
Human DDX6	Invitrogen	PA5-18478
Human Ki67-Pacific Blue (Clone KI-67)	Biolegend	350512
Cyclin D1	Cell Signaling Technology	55506
Human KRT15	invitrogen	Cat #MA5-11344
Human lfTSLP	Show Vendor	N/A
Anti Rabbit IgG-AF555	Invitrogen	A10520
Biological Samples		
Human wound punch biopsy	Duke University Health System	N/A
Chemicals, Peptides, and Recombinant Proteins		
Ghost Dye™ Violet 510	Tonbo	13-0870-T100
Recombinant mouse TSLP	R & D Biosystems	555-TSB-010
Recombinant human TSLP	Biolegend	582404
Recombinant human lfTSLP	This paper	NA
Recombinant human sfTSLP	This paper	NA
iScript cDNA Synthesis kit	Biorad	Cat# 1708891
Triton X-100	Sigma-Aldrich	T8787
ProlongGold Antifade reagent	Thermo Fisher Scientific	P36930
qPCRBIO SyGreen Blue Mix Hi-ROX	Genesee Scientific	17-507DB
Epilife Calcium Free Media	Gibco	MEPICF
Human Keratinocyte Growth Supplement (HKGS)	Gibco	S0015
TRIzol	Thermo Fisher Scientific	15596026
DNase I	VWR	IC19006210
Collagenase II	Life Technologies	17101015
Hoechst 33342	Invitrogen	H3570
0.5% Trypsin-EDTA (10x), no phenol red	Gibco	1540054
Click-iT™ Plus EdU Cell Proliferation Kit for Imaging, Alexa Fluor™ 647 dye	Invitrogen	C10640

(Z)-4-Hydroxytamoxifen	Sigma	H7904
Critical Commercial Assays		
TSLP ELISA kit (human)	Biolegend	434204
TSLP ELSIA kit (mouse)	Biolegend	434104
Experimental Models: Cell Lines		
Normal human epidermal keratinocytes (HEKa)	Gibco	C0055C
Experimental Models: Organisms/Strains		
C57BL/6J mice	Jackson Labs	Stock No: 00064
Lgr5-eGFP-IRES-creERT2	Blanche Capel, Duke University	Jax Stock No: 008875
Tslpr$^{flox/flox}$	Steven Ziegler, Benaroya Institute	N/A

Experimental Methods

1. Animal study

Female and male C57BL6/J (6-12 weeks of age; the Jackson Laboratory, Bar Harbor, ME), were used in our studies. Mice were maintained under specific pathogen-free conditions and were sustained under regulated conditions with food and water ad libitum in the pathogenic-free facility at Duke University. All mice were in the same hair cycle while in vivo experiments were performed. The protocol was approved by the Institutional of Duke University Animal Care and Use Committee under protocol A156-17-06. *Lgr5*^{CreER}*.Tslpr*$^{fl/fl}$ mice were used to study the role of TSLPR ablation in HFSCs during developmentally programmed hair growth and growth after wounding. Briefly, *Lgr5* ^{CreER} mice (kindly provided by Blanche Capel, Duke University; available from Jackson Labs, Stock #008875) (Barker et al., 2007) were crossed to *Tslpr*$^{fl/fl}$ mice (kindly provided by Stephen Ziegler, Benaroya Institute). Genotypes were validated using PCR and all experimental cohorts were co-housed; animal experiments were controlled using littermates lacking *Lgr5*^{CreER} or at least one copy of *Tslpr*^{fl}. To study the role of TSLPR in WIHG in adult mice, animals were carefully shaved and treated with 50ug 4-Hydroxytamoxifen (4OHT) (Sigma # H7904) dissolved in 100% ethanol at p46, p48, and p50. 4OHT was delivered dropwise directly to the back skin in the center of the back. Mice were then wounded at p54 in second telogen.

In vivo skin injury: 6-12-week old male and female mice were used in experiments where 4-mm diameter punch biopsy wounds or 12-mm diameter wounds were induced on the back skin of anesthetized mice. All experimental groups were in an equivalent telogen stage of the hair cycle unless otherwise stated. 4-6 full-thickness wounds were prepared paravertebrally on the back of each mouse using a punch biopsy instrument for 4mm wounds. Only one wound in the center of the back was used for 12-mm diameter excisional wounds.

Cytokine treatment: When used, recombinant murine Tslp (R&D Systems, 555-TS-010) was delivered directly to wound site in a total volume of 5µL. p50 mice in second telogen were anesthetized, shaved, and injected at tail base using 31g needle and allowed to diffuse across mouse back. Either 100uL 0.01% BSA in 1x DPBS or 250ng TSLP in 100uL total PBS was delivered; experimenters were blinded to animal groups

Hair cycle synchronization and analysis: Hair follicle synchronization and analysis of stages were based on criteria outlined in Müller-Röver et al. (Müller-Röver et al., 2001). Briefly, hair was gently depilated in defined areas on dorsal skin of mouse Mice were shaved with electric clippers when in telogen. Entry to anagen was determined by darkening of the skin and re-appearance of hair. Cycle entry into catagen was determined by pigmentation in the skin. Hair cycle progression was completed using ImageJ to quantify skin darkening (coupled to melanogenesis). Mice were checked every 2-4 days. Hair cycle phenotypes are consistently observed in both male and female mice. Mice were monitored for hair growth with were taken every 2-4 days after stimulation. Telogen' denotes telogen following a complete hair cycle. Quantification of total skin darkening and measurements of area of anagen skin was completed using ImageJ Software. When harvesting skin for subsequent analysis, scissors were used to bluntly dissect away the epidermis, dermis, and minimal subcutaneous fat from the underlying muscle. Subcutaneous fat was mechanically removed

2. Flow cytometry

To produce skin cell suspensions from whole skin, skin pieces were processed as described in (Yang et al., 2017). Skin samples collected during anagen (where stated), skin pieces were floated first on 2% Collaginase Type II for 1-2h on ice prior to floating on Trypsin GNK overnight at 4C. Epidermis was gently peeled away from dermis following incubation step. Air interface was maintained with epidermis during each step. Dermal tissue minced using surgical scissors and incubated at 37C for 1h in collagenase type II (2 mg/ml; Thermo Fisher Scientific). To produce skin cell suspensions from hair follicles, hair was gently depilated from intact skin surrounding wounds and submerged in 0.1% Trypsin GNK solution and incubated on ice for 1h with agitation to encourage physical dissociation. Solution was inactivated with equal volume keratinocyte medium containing 5% FCS and filtered through 30um filter. Epidermal cell

suspensions were prepared from dorsal skin and stained for CD45, eGFP (LGR5), CD34, and integrin α6 (ITGA6). Bulge HFSCs were defined as $CD45^{-}LGR5^{+}CD34^{+}$. Suprabasal bulge cells were identified as $ITGA6^{lo}$ and basal bulge cells were identified as $ITGA6^{hi}$. LGR5 eGFP signal amplified using anti-EGFP-AF488 (Invitrogen A-21311). Flow cytometry was performed on Canto II (BD Biosciences) and data were analyzed using FlowJo software (Treestar). Staining antibodies are listed in reagent table; Live dead staining (GhostViolet, Tonbo) was performed according to manufacturer instructions. All samples were blocked using anti CD16/32 Antibody (Biolegend) and staining was performed in FACS buffer for 40 minutes on ice.

3. Cell culture

Adult human keratinocytes (Gibco) maintained for up to 6 passages in T-75 flasks. Cells were grown in 37°C serum-free EpiLife cell culture medium (Gibco) with human keratinocyte growth supplement containing 0.05 mM Ca2+. Cells were passaged by dissociating adherent cells 0.05% Trypsin EDTA, equal volume of 1x defined trypsin inhibitor, and resuspended in complete keratinocyte medium. Media was replaced 16-24h after passaging into well plates for experiments containing recombinant human TSLP (Biolegend) at a concentration of 100 ng/mL.

4. EdU proliferation

EdU was reconstituted in sterile PBS at 10 mM concentration Thermo Fisher Scientific (MA, USA, Catalog # A10044), and stored at − 20 °C. EdU was delivered using intraperitoneal injection 3h prior to tissue collection at 20 ug/g (eg 20g mouse received 400ug EdU in 200uL PBS). Copper-catalyst based Click reaction performed according to manufacturer instructions (Invitrogen C10640, C10635) and analyzed using flow cytometry.

5. Skin explant preparation and culture.

Normal skin samples were obtained from otherwise discarded tissue of male and female patients age ~40-70 years undergoing abdominoplasty at Duke University Medical Center under protocol Pro00079799 and used in an anonymized fashion. All human samples for this study were obtained according to the protocols approved by the Institutional Review Board at Duke University. Tissue was prepared as described (Suwanpradid et al., 2017). Tissue was processed by removing adipose tissue layer and cut 1cm by 1cm by 0.5cm (depth). Tissue was placed on surgifoam to maintain epidermal-air interface in 0.5mL DMEM Dulbecco's modified Eagle's medium (DMEM) (Gibco #11054001) containing 2% FBS in 12-well tissue culture dish. To wound tissues, surgical scissors were held with blades perpendicular to tissue and 20 repeated incisions were made to tissue. Unless stated otherwise, all SOC samples were cultured for 24 hours. To separate epidermis and dermis, skin samples were floated on Trypsin GNK (0.3% trypsin/0.1% glucose, 14.8 mM NaCl, 5.3 mM KCL) (Sigma Aldrich, St. Louis, MO), for 15 minutes at 37 °C. Epidermal and dermal fractions were subsequently minced for trizol-RNA extraction.

6. Immunofluorescent staining and microscopy

Murine back and human skin wounds were excised and placed into OCT cassettes and stored at -80°C for sectioning. Antibodies used can be found in the Key Resources Table. OCT sections were cut at 9 μM were prepared as following:Human skin sections and cell culture slides were fixed using 4% PFA for 10 minutes. Tissues/cells were permeabilized with 0.1% Triton for 10 minutes. Mouse skin sections were fixed and permeabilized using Acetone at -20°C for 15 minutes. All samples were subsequently blocked for a minimum of 1h. Tissue sections were stained with a primary antibody overnight at 4°C. The following day, sections were washed stained with secondary Ab at 1:800 dilution at room temperature in the dark for 3h. After washing and adding a Hoechst stain at 1:6000 dilution, sections were mounted using Gold Anti-Fade reagent and a cover slip and imaged using the Olympus IX73 or Zeiss 780 upright confocal microscope.

7. RNA isolation, cDNA synthesis, and quantitative RT-PCR (qPCR)

Total RNA was isolated from trizol using TRIZOL reagent per the manufacturer's instructions (Invitrogen), followed by treatment with DNase I. RNA was quantified using Nanodrop 1000 or cDNA was generated

using cDNA Synthesis Kit (Bio-Rad, Hercules, CA). Amplification was detected using Fast SYBR Green Master Mix (Applied Biosystems) or sybrgreen blue (PCR biosystems) and 10-20ng cDNA used per qPCR reaction. qPCR was performed with primers as indicated in resource table. GAPDH expression was used as internal control (see primer sequences). Fold changes calculated for gene expression in human samples were normalized to donor-matched non-wounded control. *In vitro* and *in vivo* experiments were normalized to untreated or unwounded controls as indicated. Data are represented as fold change or using ddCt method as indicated. Where necessary, data were Log2 transformed to best represent the observed proportional changes.

8. Statistical analyses

Group sizes were determined based on the results of preliminary experiments without pre-determination of sample size. Preliminary experiments were performed to determine requirements for sample size, considering resources available and ethical, reductionist animal use. Mice were randomly assigned to groups. Mouse studies were not performed in a blinded fashion. Statistical analysis using the two-tailed unpaired Student's t test, under the untested assumption of normality, was calculated using Prism software (GraphPad) unless specified otherwise. A *p*-value of <0.05 was considered statistically significant. where $p<0.01$ **, $p<0.001$***, $p<0.0001$ ****. Error bars represent ± SEM.

9. Protein quantification and ELISA

Total protein was extracted from mouse tissue with Pierce RIPA Buffer (ThermoScientific) with proteinase inhibitor cocktail (EDTA-free, Roche). Protein concentration was determined using DC protein assay. TSLP mouse ELISA kit was used to determine the amount of TSLP according to manufacturer instructions.

10. Microarray and RNA Sequencing analysis

The mouse microarray data from Christmann et al. (GSE34297) and the skin samples from Chen et al. (GSE23006) were each normalized independently by the robust multichip average (RMA) approach to eliminate systematic differences across the arrays using the affy (Gautier et al., 2004) bioconductor (Huber et al., 2015) package from the R statistical programming environment. Differential expression between skin treated with subcutaneous TSLP or vehicle was carried out using the limma (Ritchie et al., 2015) package.

The RNA-sequencing dataset from Iglesias-Bartolome et al. (GSE97615) contained samples from human axillary skin wounds at baseline (Day 1, unwounded), two days after full-thickness 3-mm punch biopsy wounding (Day 3), and five days after wounding (Day 6) (Iglesias-Bartolome et al., 2018). The raw data was downloaded and processed using the fastp toolkit (Chen et al., 2018) to trim low-quality bases and Illumina sequencing adapters from the 3' end of the reads. Only reads that were 20nt or longer after trimming were kept for further analysis. Reads were mapped to the GRCh38v93 version of the human genome and transcriptome (Kersey et al., 2012)using the STAR RNA-seq alignment tool (Dobin et al., 2013). Reads were kept for subsequent analysis if they mapped to a single genomic location. Gene counts were compiled using the featureCounts tool (Liao et al., 2014). Only genes that had at least 10 reads in any given library were used in subsequent analysis. This resulted in a set of 12 samples and 23,378 genes. Normalization and differential expression between Day 6 and Day 1, as well as Day 3 and Day 1, was carried out using the DESeq2(Love et al., 2014) bioconductor (Huber et al., 2015) package with the R statistical programming environment. The p-values were corrected for multiple hypothesis testing by the Benjamini-Hochberg method. A gene was considered downregulated if it had an adjusted p-value <= 0.05 and a negative fold-change in either the Day 3-vs-Day 1 analysis or the Day 6-vs-Day 1 analysis. Likewise, a gene was considered upregulated if it was significant in either comparison along with a negative fold-change.

11. Data availability

We used the publicly available microarray datasets from Christmann et al. (GSE34297), Chen,et al (GSE23006) and the RNA-seq data set from Iglesias-Bartolome et al. (GSE97615).

12. lfTSLP pAb design overview (AbClonal):

Synthesized and subcloned target TSLP gene (130 amino acids) to bacterial expression vector and expressed protein for use as antigen. Additional peptide expression for positive purification using specific fragment (DFTNCDFEKIKAAYLSTISKDLITYMSGTKSTEFNNTVSCSNRPHCLTEIQSLTFNPTAGCASLAKE) And negative purification of sfTSLP non-specific peptide. The antibody was designed to only target the specific fragment using cross purification.

Protein expression and purification

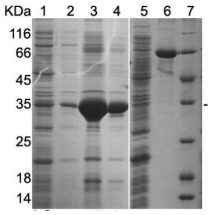

1. Supernatant
2. Supernatant 2 (2M Urea dissolved inclusion bodies)
3. Inclusion body diluted in 2 folds (BM Urea dissolved inclusion bodies)
4. Inclusionbody diluted in 10 folds (BM Urea dissolved inclusion bodies)
5. pET-28a-SUMO Empty Induced expression
6. 0.4mg/ml BSA
7. Marker

pET-28a-SUMO-TSLP (29-159aa) was expressed as inclusion bodies. The inclusion body protein was 6 mg/mL concentration, so it was used for immunization.

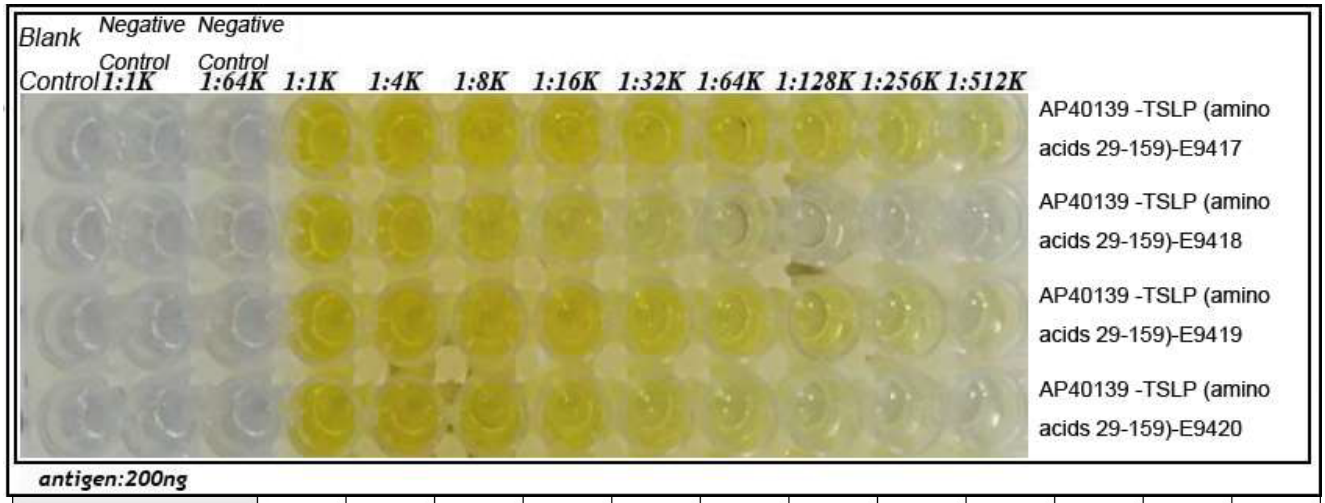

AP40139 TSLP(amino acids 29-159)	Blank	Negative Control 1:1K	Negative Control 1:64K	Positive 1:1K	Positive 1:4K	Positive 1:8K	Positive 1:16K	Positive 1:32K	Positive 1:64K	Positive 1:128K	Positive 1:256K	Positive 1:512K
E9417	0.0572	0.0706	0.0448	1.2151	1.1926	1.092	1.0601	0.9799	0.8327	0.6875	0.53	0.3562
E9418	0.0408	0.0522	0.0949	1.1581	0.9756	0.7896	0.5984	0.3966	0.2729	0.1604	0.1406	0.0912
E9419	0.05	0.0532	0.0503	1.2408	1.1013	0.988	0.9279	0.7677	0.5735	0.4393	0.3118	0.2011
E9420	0.0354	0.0397	0.0366	1.1919	0.999	0.8687	0.7286	0.5332	0.3528	0.2242	0.1686	0.1117

ELISA

Immunization schedule

Immunization	Day	Date	Dose	Adjuvant	Animal status
1st	1	2018/12/07	0.3mg	CFA	Good
2nd	12	2018/12/19	0.15mg	IFA	Good
3rd	26	2019/01/02	0.15mg	IFA	Good
4th	40	2019/01/06	0.15mg	IFA	Good
Serum Collection	52	2019/01/28			Normal

Antisera were purified by the specific fragment (peptide 1) and the non-specific fragment (peptide 2).

Antibody concentrations
E9417(P) Conc.:0.58mg/mL; E9417(C) Conc.:0.59mg/mL
E9418(P) Conc.:0.34mg/mL; E9418(C) Conc.:0.32mg/mL
E9419(P) Conc.:0.90mg/mL; E9419(C) Conc.:0.27mg/mL
E9420(P) Conc.:0.33mg/mL; E9420(C) Conc.:0.18mg/mL

Sensitivity:

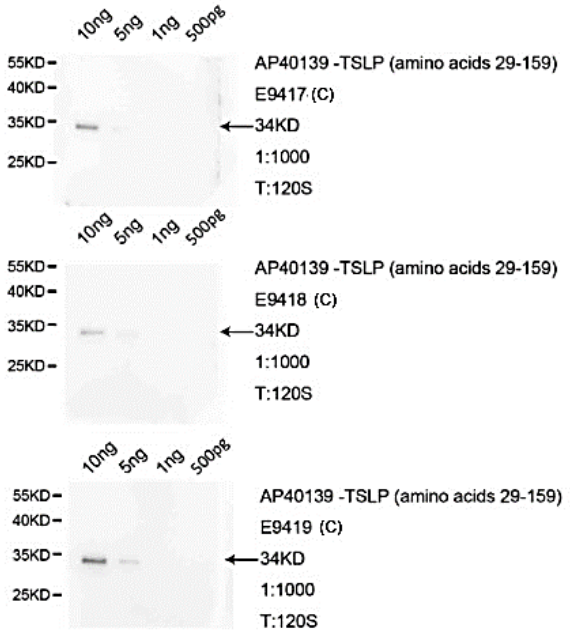

Note: Lanes one through four were loaded with 10ng, 5ng, 1ng, and 500pg of antigen, respectively.
The antibodies are in a 1:1000 dilution ratio

Analysis:

- Bands of 34KD were observed for E9417(C), E9418(C), and E9419(C), consistent with the expected molecular weight.
- 10ng of Ag can be detected by antibodies E9417(C), E9418(C)
- 5ng of Ag can be detected by antibodies E9419(C)

E9419(C) used for immunostaining as described (1:400 dilution)

References

Abbasi, S., and Biernaskie, J. (2019). Injury modifies the fate of hair follicle dermal stem cell progeny in a hair cycle-dependent manner. Experimental Dermatology *28*, 419-424.

Aran, S., Zahri, S., Asadi, A., Khaksar, F., and Abdolmaleki, A. (2020). Hair follicle stem cells differentiation into bone cells on collagen scaffold. Cell and Tissue Banking.

Barker, N., van Es, J.H., Kuipers, J., Kujala, P., van den Born, M., Cozijnsen, M., Haegebarth, A., Korving, J., Begthel, H., Peters, P.J*., et al.* (2007). Identification of stem cells in small intestine and colon by marker gene Lgr5. Nature *449*, 1003-1007.

Blanpain, C., and Fuchs, E. (2014). Plasticity of epithelial stem cells in tissue regeneration. Science *344*, 1242281.

Blanpain, C., Lowry, W.E., Geoghegan, A., Polak, L., and Fuchs, E. (2004). Self-Renewal, Multipotency, and the Existence of Two Cell Populations within an Epithelial Stem Cell Niche. Cell *118*, 635-648.

Chen, S., Zhou, Y., Chen, Y., and Gu, J. (2018). fastp: an ultra-fast all-in-one FASTQ preprocessor. Bioinformatics *34*, i884-i890.

Cotsarelis, G., Sun, T.-T., and Lavker, R.M. (1990). Label-retaining cells reside in the bulge area of pilosebaceous unit: Implications for follicular stem cells, hair cycle, and skin carcinogenesis. Cell *61*, 1329-1337.

Dobin, A., Davis, C.A., Schlesinger, F., Drenkow, J., Zaleski, C., Jha, S., Batut, P., Chaisson, M., and Gingeras, T.R. (2013). STAR: ultrafast universal RNA-seq aligner. Bioinformatics *29*, 15-21.

Gautier, L., Cope, L., Bolstad, B.M., and Irizarry, R.A. (2004). affy--analysis of Affymetrix GeneChip data at the probe level. Bioinformatics *20*, 307-315.

Gay, D., Kwon, O., Zhang, Z., Spata, M., Plikus, M.V., Holler, P.D., Ito, M., Yang, Z., Treffeisen, E., Kim, C.D*., et al.* (2013). Fgf9 from dermal γδ T cells induces hair follicle neogenesis after wounding. Nature Medicine *19*, 916-923.

Ge, Y., Gomez, N.C., Adam, R.C., Nikolova, M., Yang, H., Verma, A., Lu, C.P.-J., Polak, L., Yuan, S., Elemento, O*., et al.* (2017). Stem Cell Lineage Infidelity Drives Wound Repair and Cancer. Cell *169*, 636-650.e614.

Greco, V., Chen, T., Rendl, M., Schober, M., Pasolli, H.A., Stokes, N., dela Cruz-Racelis, J., and Fuchs, E. (2009). A Two-Step Mechanism for Stem Cell Activation during Hair Regeneration. Cell Stem Cell *4*, 155-169.

Handjiski, B.K., EichmÜLler, S., Hofmann, U., Czarnetzki, B.M., and Paus, R. (1994). Alkaline phosphatase activity and localization during the murine hair cycle. British Journal of Dermatology *131*, 303-310.

Hsu, S., Papp, K.A., Lebwohl, M.G., Bagel, J., Blauvelt, A., Duffin, K.C., Crowley, J., Eichenfield, L.F., Feldman, S.R., Fiorentino, D.F.*, et al.* (2012). Consensus guidelines for the management of plaque psoriasis. Arch Dermatol *148*, 95-102.

Huber, W., Carey, V.J., Gentleman, R., Anders, S., Carlson, M., Carvalho, B.S., Bravo, H.C., Davis, S., Gatto, L., Girke, T.*, et al.* (2015). Orchestrating high-throughput genomic analysis with Bioconductor. Nature Methods *12*, 115-121.

Iglesias-Bartolome, R., Uchiyama, A., Molinolo, A.A., Abusleme, L., Brooks, S.R., Callejas-Valera, J.L., Edwards, D., Doci, C., Asselin-Labat, M.-L., Onaitis, M.W.*, et al.* (2018). Transcriptional signature primes human oral mucosa for rapid wound healing. Science Translational Medicine *10*, eaap8798.

Ishida, Y., Gao, J.-L., and Murphy, P.M. (2008). Chemokine Receptor CX3CR1 Mediates Skin Wound Healing by Promoting Macrophage and Fibroblast Accumulation and Function. The Journal of Immunology *180*, 569-579.

Ito, M., Yang, Z., Andl, T., Cui, C., Kim, N., Millar, S.E., and Cotsarelis, G. (2007). Wnt-dependent de novo hair follicle regeneration in adult mouse skin after wounding. Nature *447*, 316-320.

Jaks, V., Barker, N., Kasper, M., van Es, J.H., Snippert, H.J., Clevers, H., and Toftgård, R. (2008). Lgr5 marks cycling, yet long-lived, hair follicle stem cells. Nature Genetics *40*, 1291-1299.

Joost, S., Jacob, T., Sun, X., Annusver, K., La Manno, G., Sur, I., and Kasper, M. (2018). Single-Cell Transcriptomics of Traced Epidermal and Hair Follicle Stem Cells Reveals Rapid Adaptations during Wound Healing. Cell Reports *25*, 585-597.e587.

Kersey, P.J., Staines, D.M., Lawson, D., Kulesha, E., Derwent, P., Humphrey, J.C., Hughes, D.S., Keenan, S., Kerhornou, A., Koscielny, G.*, et al.* (2012). Ensembl Genomes: an integrative resource for genome-scale data from non-vertebrate species. Nucleic Acids Res *40*, D91-97.

Li, J., Chen, Y., Xu, X., Jones, J., Tiwari, M., Ling, J., Wang, Y., Harismendy, O., and Sen, G.L. (2019). HNRNPK maintains epidermal progenitor function through transcription of proliferation genes and degrading differentiation promoting mRNAs. Nature Communications *10*, 4198.

Liao, Y., Smyth, G.K., and Shi, W. (2014). featureCounts: an efficient general purpose program for assigning sequence reads to genomic features. Bioinformatics *30*, 923-930.

Lopez-Pajares, V., Yan, K., Zarnegar, B.J., Jameson, K.L., and Khavari, P.A. (2013). Genetic pathways in disorders of epidermal differentiation. Trends in Genetics *29*, 31-40.

Love, M.I., Huber, W., and Anders, S. (2014). Moderated estimation of fold change and dispersion for RNA-seq data with DESeq2. Genome Biol *15*, 550.

Müller-Röver, S., Foitzik, K., Paus, R., Handjiski, B., van der Veen, C., Eichmüller, S., McKay, I.A., and Stenn, K.S. (2001). A Comprehensive Guide for the Accurate Classification of Murine Hair Follicles in Distinct Hair Cycle Stages. Journal of Investigative Dermatology *117*, 3-15.

Ritchie, M.E., Phipson, B., Wu, D., Hu, Y., Law, C.W., Shi, W., and Smyth, G.K. (2015). limma powers differential expression analyses for RNA-sequencing and microarray studies. Nucleic Acids Res *43*, e47.

Schomann, T., Iljas, J.D., Que, I., Li, Y., Suidgeest, E., Cruz, L.J., Frijns, J.H.M., Chan, A., Löwik, C.M.W.G., Huisman, M.A.*, et al.* (2020). Multimodal imaging of hair follicle bulge-derived stem cells in a mouse model of traumatic brain injury. Cell and Tissue Research.

Segre, J.A., Bauer, C., and Fuchs, E. (1999). Klf4 is a transcription factor required for establishing the barrier function of the skin. Nature Genetics *22*, 356-360.

Stenn, K.S., and Paus, R. (2001). Controls of Hair Follicle Cycling. Physiological Reviews *81*, 449-494.

Suwanpradid, J., Holcomb, Z.E., and MacLeod, A.S. (2017). Emerging Skin T-Cell Functions in Response to Environmental Insults. J Invest Dermatol *137*, 288-294.

Wang, X., Chen, H., Tian, R., Zhang, Y., Drutskaya, M.S., Wang, C., Ge, J., Fan, Z., Kong, D., Wang, X.*, et al.* (2017). Macrophages induce AKT/β-catenin-dependent Lgr5+ stem cell activation and hair follicle regeneration through TNF. Nature Communications *8*, 14091.

Wang, Y., Arribas-Layton, M., Chen, Y., Lykke-Andersen, J., and Sen, George L. (2015). DDX6 Orchestrates Mammalian Progenitor Function through the mRNA Degradation and Translation Pathways. Molecular Cell *60*, 118-130.

Weidinger, S., Illig, T., Baurecht, H., Irvine, A.D., Rodriguez, E., Diaz-Lacava, A., Klopp, N., Wagenpfeil, S., Zhao, Y., Liao, H.*, et al.* (2006). Loss-of-function variations within the filaggrin gene predispose for atopic dermatitis with allergic sensitizations. Journal of Allergy and Clinical Immunology *118*, 214-219.

Yang, B., Suwanpradid, J., Sanchez-Lagunes, R., Choi, H.W., Hoang, P., Wang, D., Abraham, S.N., and MacLeod, A.S. (2017). IL-27 Facilitates Skin Wound Healing through Induction of Epidermal Proliferation and Host Defense. J Invest Dermatol *137*, 1166-1175.